



**Politecnico  
di Torino**



---

# SURFACE ENERGY CHARACTERIZATION

---

Characterization of Surface Energy of Chalks using Atomic Force Microscopy,  
Contact Angle Goniometry, and Crack Propagation Techniques



Presented By:

Rachid Ismail

Supervisors:

Chiara Deangeli

Christian David

Alae El-Haitami

Davide Geremia

# Abstract

This project was set-up in order to try and define the different types of surface energy while actively determining these energies for our two different chalks, and under different conditions, and verifying them. The identified values of surface energies were based on different kinds of measurements and tests on specifically prepared samples for each test. The Surface Free Energy measurements were done using Contact Angle Goniometry, which required specially prepared saturated samples to overcome the porosity effects as well as the application of a specific Model, and using Atomic Force Microscopy by identifying the Adhesion force distribution on the surface of the samples. The Surface Fracture Energy was calculated based on a Crack Propagation test dependent on the mechanical properties of the samples. These values were calculated in dry and under saturated/wet conditions in order to study the effect of the interaction of the liquids used on the surface energies and hence the mechanical properties, for the Surface Fracture Energy, and the intrinsic surface properties, for the Surface Free Energy.

Keywords: [Surface Energy]-[AFM]-[O.W.R.K]-[SCB]-[Crack Propagation]-[Fracture Energy]-[Surface Free Energy]-[Contact Angle]-[Chalk]-[Calcite]-[Obourg]-[Ciply]

# Résumé

Ce projet a été mis en place afin d'essayer de définir les différents types d'énergie de surface tout en déterminant activement ces énergies pour nos deux différentes craies, et dans différentes conditions, et en les vérifiant. Les valeurs identifiées des énergies de surface étaient basées sur différents types de mesures et de tests sur des échantillons spécifiquement préparés pour chaque test. Les mesures de l'énergie libre de surface ont été effectuées à l'aide de la goniométrie de l'angle de contact, qui a nécessité des échantillons saturés spécialement préparés pour surmonter les effets de porosité ainsi que l'application d'un modèle spécifique, et à l'aide de la microscopie à force atomique en identifiant la distribution de la force d'adhésion sur la surface des échantillons. L'énergie de fracture de surface a été calculée sur la base d'un test de propagation de fissure dépendant des propriétés mécaniques des échantillons. Ces valeurs ont été calculées à sec et dans des conditions saturées/humides afin d'étudier l'effet de l'interaction des liquides utilisés sur les énergies de surface et donc les propriétés mécaniques, pour l'énergie de rupture de surface, et les propriétés intrinsèques de la surface, pour l'énergie libre de surface.

Mots Clés : [Énergie de Surface]-[AFM]-[O.W.R.K]-[SCB]-[Propagation des Fissures]-[Énergie de Rupture]-[Énergie Libre de surface]-[Angle de Contact]-[Craie]-[Calcite]-[Obourg]-[Ciply]

# Acknowledgements

I would like to start by recognizing all the effort was put in during the work on this project by the staff members of CYU and specifically the GEC and LPPI, whose aid help make these past six months an enriching experience for me both on personal and scientific levels, as well as the I-MAT Federation who financed this internship.

I would like to thank first of all my direct supervisors for this project Professor Christian DAVID, Professor Alae EL-HAITAMI, and PhD student Davide GEREMIA who provided me with the expertise and means necessary to fulfil my duty to the maximum possible and more.

Every part of these last six months will be treasured by me eternally, from the help to develop the work-ethic mentality that had driven me for this work, to constant advice, and to those little afternoon chats that were maybe not always very scientific.

To Davide, with whom most of my work and time was, grazie mille! Con il tuo aiuto, sono riuscito a raggiungere i miei obiettivi, e anche a migliorare il mio italiano, come lingua e come cultura, nel frattempo.

To Alae, thank you for helping me, and constantly giving me advice that transcends simple work, and actually helps me become a better person and helps me find the right path for my future.

To Christian, thank you for the very rich experience that you were sharing which has changed the way I view everyday objectives in life!

I would also like to appreciate all the help I received during these months from other colleagues in the GEC laboratory, namely PhD student Anthony as well as other interns like Mahdi, Ahmed, Asma, and Kenza, which really made life easier and fun during work-hours (Table-Tennis in the breaks was a blast!).

I would also like to thank all the professors at Politecnico di Torino and the Lebanese University Faculty of Engineering who helped provide the steppingstone for me to reach the level I am at now as not only an engineer, but also as a human being. In those means, I would like to mention my supervisor for this project from Politecnico di Torino, Professor Chiara DEANGELI, as well as the heads of departments Joyce KHEIR from the Petrochemical Engineering department in the Lebanese University, and Professor Laura Valentina Socco from DIATI in PoliTo.

Last but not least, I would like to thank my family and friends who have been with me on this journey that spanned five years, and three countries. You guys made every step of the way seem like the best and have made contributions and memories that I will hold dearly with me for the rest of my life.

# Table of Contents

Abstract.....	0
Résumé .....	0
Acknowledgements .....	1
List of Tables.....	5
List of Charts.....	6
List of Graphs.....	6
List of Figures.....	6
Introduction .....	1
1. Theoretical Background .....	2
1.1. Surface Free Energy.....	2
1.2. Fracture Surface Energy.....	3
1.3. Surface Energy Alteration .....	3
2. Methodology .....	6
2.1. Samples.....	6
2.2. Advancing Angle Measurements.....	18
2.3. O.W.R.K Model.....	26
2.4. O.W.R.K Model with Calcites .....	32
2.5. SCB & Fracture Toughness .....	33
2.6. Brine Contact Angle Measurements on Calcites.....	44
2.7. SFE With AFM.....	45
3. Results .....	56
3.1. O.W.R.K Model on Chalk.....	56
3.2. O.W.R.K Model on Calcite.....	63
3.3. SCB.....	65
3.4. Brine Contact Angle Measurements on Calcites.....	69

3.5. AFM .....	71
4. Discussion .....	72
5. Conclusion .....	74
References.....	75
Appendices.....	

# *List of Tables*

Table 1- Obourg and Cibly Chalks' Characteristics .....	8
Table 2- Different Resins Produced by Struers .....	16
Table 3- Mean Value of Contact Angle Measurements on Different Resins .....	17
Table 4- Sample Liquids' Properties.....	30
Table 5- Recommended Geometrical Dimensions of SCB Specimen .....	37
Table 6- Salinity of the Used Brines .....	44
Table 7- NanoElectrical Lab – Techniques and Applications .....	49
Table 8- Mean Contact Angle Values of Ultra-Pure Water.....	56
Table 9- Mean Contact Angle Values on Pure Resin Samples.....	57
Table 10- Average and Standard Deviation Values of all Contact Angle Measurements Including Porosity..	58
Table 11- Roughness Measurement of Chalks .....	59
Table 12- The Cosine of the Contact Angle on the Pure Chalk.....	59
Table 13- Final O.W.R.K Model Calculations for Obourg Chalk .....	60
Table 14- SFE of Obourg Chalk .....	61
Table 15- Final O.W.R.K Model Calculations for Cibly Phosphatic Chalk.....	61
Table 16- SFE of Cibly Phosphatic Chalk.....	62
Table 17- Average and Standard Deviation Values of Contact Angle Measurements on Calcite .....	63
Table 18- Roughness Measurements of Calcites .....	63
Table 19- Final O.W.R.K Model Calculations for Calcite .....	63
Table 20- Porosity Measurements for Obourg SCB Samples .....	66
Table 21- UCTs.....	67
Table 22- $K_{Ic}$ and $\gamma$ Values for Cibly Phosphatic Chalk.....	67
Table 23- $K_{Ic}$ and $\gamma$ Values for Obourg Chalk .....	68
Table 24- Literature Surface Energy Results of Calcites .....	68
Table 25- Average Values of Contact Angle Measurements for Each Brine .....	69
Table 26- AFM SFE.....	71
Table 27- Surface Energy .....	72
Table 28- Contact Angle Measurements on Calcites .....	App
Table 29- Contact Angle Measurements on Phosphatic Cibly Chalk .....	App
Table 30- Contact Angle Measurements on Pure Resin.....	App
Table 31- Contact Angle Measurements on Obourg Chalk.....	App
Table 32- Brine Static Contact Angle Measurements on Calcites .....	App
Table 33- SCB Tests on Cibly Phosphatic Chalk .....	App

Table 34- SCB Tests on Obourg Chalk.....	App
--	-----

## *List of Charts*

Chart 1- Contact Angle Values of Ultra-Pure Water .....	56
Chart 2- Contact Angle Values of Sample Liquids on Pure Resin .....	57
Chart 3- Obtained Means* of the Advancing Angle Measurements .....	58

## *List of Graphs*

Graph 1- O.W.R.K Model.....	31
Graph 2- UCT.....	42
Graph 3- Stress Vs Strain.....	43
Graph 5- O.W.R.K Model for Obourg Chalk.....	60
Graph 6- O.W.R.K Model for Ciplly Phosphatic Chalk .....	62
Graph 7- O.W.R.K Model for Calcite.....	64
Graph 8- Contact Angle Measurements vs. Ionic Strength for NaCl and MgCl <sub>2</sub> Brines in Calcites .....	69

## *List of Figures*

Figure 1- Ekofisk Subsidence .....	4
Figure 2- The Mons Basin in Belgium in which we have the Ciplly and Obourg Quarries .....	6
Figure 3- Transversal Schematic Profile of the Mons Basin .....	7
Figure 4- SEM Graphs on Chalks .....	8
Figure 5- Cored Chalk Blocks .....	9
Figure 6- Diamond Drill Coring Machine .....	9
Figure 7- Chalk Sample Preparation .....	10
Figure 8- Droplet Absorption.....	11
Figure 9- EpoFix & Hardener .....	11
Figure 10- Vacuum Chamber .....	12
Figure 11- A Resin Block Filled with Samples .....	14
Figure 12- Remaining Layer of Resin.....	15
Figure 13- Arrival at an Unsaturated Level within the Sample .....	15
Figure 14- Prepared and Hardened Samples of CaldoFix-2, LevoCit, and SpeciFix-40 (From Left to Right)	17

Figure 15- Difference in Penetration between the Previous and Final Method of Preparation .....	17
Figure 16- Goniometer Simplified Set Up.....	18
Figure 17- Measurement Procedures, and Variables Controlling the Quality of Measurements.....	19
Figure 18- The CLSM.....	20
Figure 19- Autofluorescence of Different Materials in our Samples.....	21
Figure 20- The CLSM Roughness Measurement.....	21
Figure 21- Dynamic Contact Angle Measurement .....	24
Figure 22- Dynamic Contact Angles.....	25
Figure 23- A Few Resin and Saturated Rock Samples.....	25
Figure 24- Components of the Young's Equation .....	26
Figure 25- Schematic Representation of the Two-Component Phase Contact Mode without Compatibility ..	28
Figure 26- Schematic Representation of the Two-Component Phase Contact Mode with Compatibility .....	28
Figure 27- Sample Liquids: Formamide - Diiodomethane - DMSO - Glycerol - Ultra-Pure Water.....	30
Figure 28- A Translucent Calcite.....	32
Figure 29- DTT Set-up.....	33
Figure 30- Crack Propagation Tests.....	34
Figure 31- SCB Set-up.....	35
Figure 32- Creating the Notch with a Saw .....	36
Figure 33- SCB Geometry Parameters .....	36
Figure 34- Precise Cutting Machine.....	38
Figure 35- UCT with Evident Failure .....	40
Figure 36- Saturation Process .....	40
Figure 37- Immersed Mass Measurement .....	41
Figure 38- AFM.....	45
Figure 39- High-Resolution Imaging using Contact Mode .....	46
Figure 40- Delicate and Accurate Imaging using the Tapping Mode .....	46
Figure 41- Frequency Used for Different Nanomechanical Modes.....	47
Figure 42- Nanoscale Resolution Imaging using QNM .....	47
Figure 43- AFM-nDMA Imaging .....	48
Figure 44- Topography (Left) and Tunneling (Right) Images of an 8.5 nm-Thick SiO <sub>2</sub> Sample.....	49
Figure 45- PeakForce Tapping Pattern.....	51
Figure 46- JKR VS DMT .....	52
Figure 47- In Fluid Imaging Probe.....	53
Figure 48- Sketch Representing In Fluid AFM Measurement.....	53
Figure 49- PeakForce QNM Visualized Using the NanoScope Analysis 2.0 Software .....	55
Figure 50- Roughness Measurements of OB Chalk Sample 1.....	App

Figure 51- Roughness Measurements of OB Chalk Sample 2..... App  
Figure 52- Roughness Measurements of PH Chalk Sample 1 ..... App  
Figure 53- Roughness Measurements of PH Chalk Sample 2 ..... App  
Figure 54- Roughness Measurements of Calcite 1..... App  
Figure 55- Roughness Measurements of Calcite 2..... App

# Introduction

Surface Energy characterization is used for multiple industries all around the world, mainly for industrial and chemical manufacturing purposes.

We can find in the literature multiple sources measuring the Surface Free Energy of polymers to study the quality of their processes, or measuring the Surface Fracture Energy of certain minerals or metals, while calling both Surface Energies.

It is important to understand the difference between the two terms, as they are not the same and correspond to completely different values.

There are multiple methods, models, and devices used to calculate the surface energies, including Atomic Force Microscopy (AFM) as well as Contact Angle Goniometry for the Surface Free Energy, and such as the crack propagation methods for the Surface Fracture Energy.

What we intended on doing in this project is try and find both kinds of surface energies for our chalk samples, to compare them and have a better understanding of the difference between them. Moreover, we would like to test the water-weakening effects that impact reservoirs during waterflooding operations through these surface energy calculations and check the influence of having different ions in the solutions used to study this effect.

# 1. Theoretical Background

Many different theories have been set out to try and explain the phenomena witnessed on the surfaces of any and every material. There could be many contributing factors depending on the studied phenomena, most of which have effects on multiple aspects, be it chemical or physical.

When studying the surface of samples, the first parameter that comes to mind is the geometry (and on a smaller scale the roughness), and the geometry alone truly plays an incredible part on every aspect. Nonetheless, looking at intrinsic characteristics of every material, the first idea should be knowing what these materials are made from. As such the effect of dropping a droplet of water on a gold film, will always be different to dropping it on a chalk disk. Likewise, breaking a wooden spoon is never the same as propagating a fracture in a sandstone.

These last two examples mainly depend on one parameter (or perhaps two): Surface Energy.

Surface Energy has multiple definitions in the literature, mainly depending on the field in which it is being used or calculated.

## 1.1. Surface Free Energy

Surface Free Energy (SFE) is the free energy available on the surfaces of materials. And free energy as thermodynamically defined, refers to the energy that is accessible to do work.[1]

The SFE is rather evident by the interactions that happen at that surface. To understand these interactions, we should imagine a single molecule in a drop of liquid. This molecule is surrounded by a homogeneous environment and will be subjected to cohesive force from adjacent molecules, causing the molecule to tend to stay in the bulk. As we advance towards the surface of the liquid where it is in contact with another phase, the molecule will be subjected to cohesive forces toward the bulk but also some weaker adhesive forces towards the adjacent phase. This results in a net attraction into the bulk that tends to reduce the number of molecules at the surface and to increase the intermolecular space between the surface molecules. The increased separation requires energy, same as in the case of stretching a spring, and this excess energy results in the surface tension and the Surface Free Energy.[2]

The SFE can be referred to as the (thermodynamically unfavorable) energy of making "dangling bonds" at the surface. This is the reason for the availability of establishing adhesive forces at the surface. Atoms at the surface are under-coordinated, and because it costs energy to break bonds, surface atoms always have superior energy than atoms in the bulk. This happens regardless of the type of bond, be it covalent (as in a metal), ionic (in a salt), or non-covalent (in a liquid such as water).[3]

Controlling the SFE of materials means controlling the interactions that happen on our surfaces and understanding how they react with the different fluids that they come in contact with.

## 1.2. Fracture Surface Energy

The fracture surface energy, also known as the fracture energy, can basically be defined as the work required per unit area to create new surface.[4]

The measurement of this kind of surface energy is usually done based off crack propagation experimentation. The first step towards the formation and propagation of cracks is the formation of a single nano-crack, which when accumulated, will form the macroscopic cracks. Early nano-cracks are usually the result of an external load application, and they start forming at stresses which are stress as low as one third of the load bearing capacity. With increasing load, we have the formation of more and more cracks, as well as an increase in the lengths of the existing ones, which will induce damage to the material. This damage can be observed either by increased capillary absorption, or by the gradual decrease of the stiffness. Once we arrive at the maximum stress, the damage induced is too big and the density of the nano-cracks is too high that the material starts to develop micro-cracks. After that we will have an accumulation of micro- and nano-cracks at in the so-called fracture process zone which will be the place where the macro-cracks eventually form. Hence, the energy required to form a macro-crack is the sum of all nano-cracks which are necessary to be formed before failure.[5][6][7]

## 1.3. Surface Energy Alteration

Having the ability to control the surface is very important to many different sectors, for whom the interactions happening at the surface are of extreme importance. For example, knowing and controlling the interaction between different types of ink will with regular papers can help

manufacturers enhance their production quality and choose the most suitable type. Nonetheless, the alteration of surface energies goes beyond industries is currently targeted in the Oil & Gas domain as understanding the surface interactions between different solids and fluids, or in this case between rocks and brines for examples, is of extreme importance.

To have this kind of control depends on the methodology used to alter the surface energy values, both the fracture and the free surface energies.

For each fluid coming into contact with a certain surface, the interaction will be completely different; likewise, changing the material and encountering it with the same fluid will have completely different results. This depends the surface energies of each material and how they react to each fluid based on multiple properties that depend on both phases. As a fluid comes in contact with a surface, it is actually occupying some of the “dangling bonds” left at the surface thus reducing the “excess” amount and altering the overall value.

In terms of the Oil & Gas sector, brine interactions with the reservoir rocks during waterflooding for example, will have a certain effect on the surface energy of these rocks. Decreasing this energy means easier and higher probability of fractures, which for example can enhance our secondary porosity, or it can cause grain crushing and thus a lower porosity.

This is why it is of utmost importance that we understand these interactions and try to manipulate them to enhance the production.

In the literature we can find already find multiple theories mentioning the phenomenon known as water-weakening, which basically describes the weakening effects of water on rock structures. It is very clearly visible for example in the Ekofisk reservoir in the North Sea.

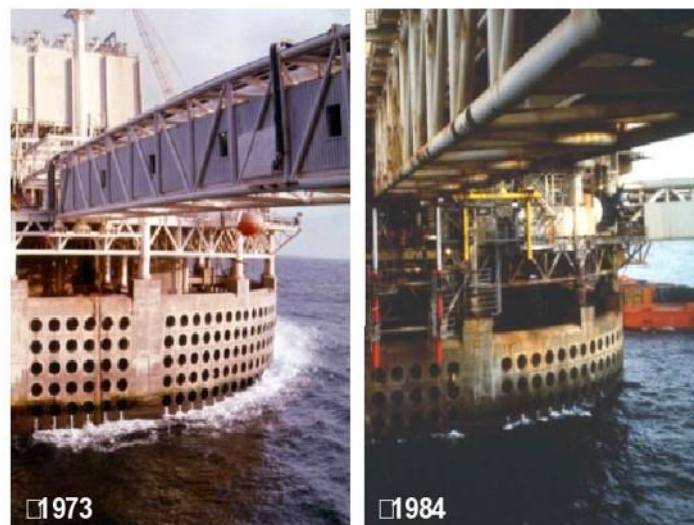


Figure 1- Ekofisk Subsidence

The Ekofisk Oil Field was subjected to about ten feet of subsidence over one decade as is evident in *Figure 1*. This caused a huge drive towards understanding the factors that lead to such results, of which water-weakening can be attributed.

Of the many theories set out to explain this phenomenon, the effect that the surface energy plays appears to be the most effective.

This is why we decided to do some experiments that would test the credibility of this theory and check if water interaction, or perhaps weakening, can be viewed in terms of changes in the surface energy.

## 2. Methodology

Out of all available theories, we were mainly interested in testing the surface energy hypothesis, as we believe that it can lead to some unprecedented results in terms of the understanding of the water weakening phenomenon. So basically, our goal was to create the perfect conditions to understand the role that the surface energy plays in terms of the water weakening.

### 2.1. Samples

In order to test any theory, the most important thing is preparing an adequate sample that can best model the hypothesis that we intend to study. Our goal being to study effect of water weakening on carbonate rocks, like in chalk reservoirs.

The two types of chalk we have been working on are both from the Mons Basin (*Figure 1*) in Belgium, namely from quarries producing the Ciply and Obourg chinks. Big blocks were excavated from these quarries to use a resource of material for our studies.

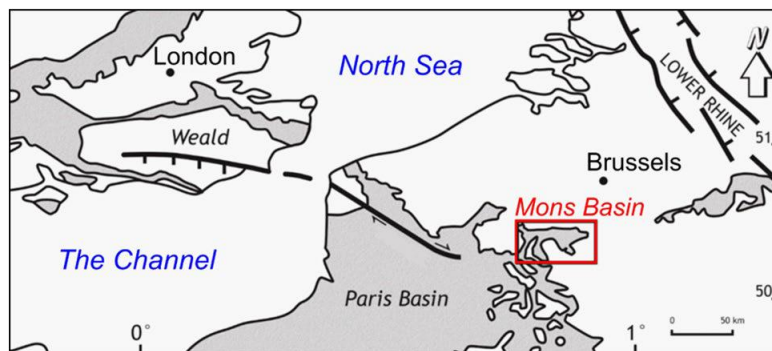


Figure 2- The Mons Basin in Belgium in which we have the Ciply and Obourg Quarries[12]

The Mons Basin is a rather small, yet special subsiding zone mainly originating from deep outcrop formation processes. It is basically a gentle syncline defined by the extension area of Cretaceous-Cenozoic sediments that accumulated within an east-west subsiding zone in Belgium, near the Paris Basin, to which it is connected westward. The subsiding area is relatively small, extending less than 40 km by 15 km in dimension, and having a maximum depth of only 300 m. However, the Mons Basin is interesting to geologists because it has a significantly different sedimentary record from that

of other nearby basins, such as the Paris Basin. In addition, the basin has a unique structure whereby for each sedimentary unit, the maximum thickness is found in a different region of the basin. [8];[9]

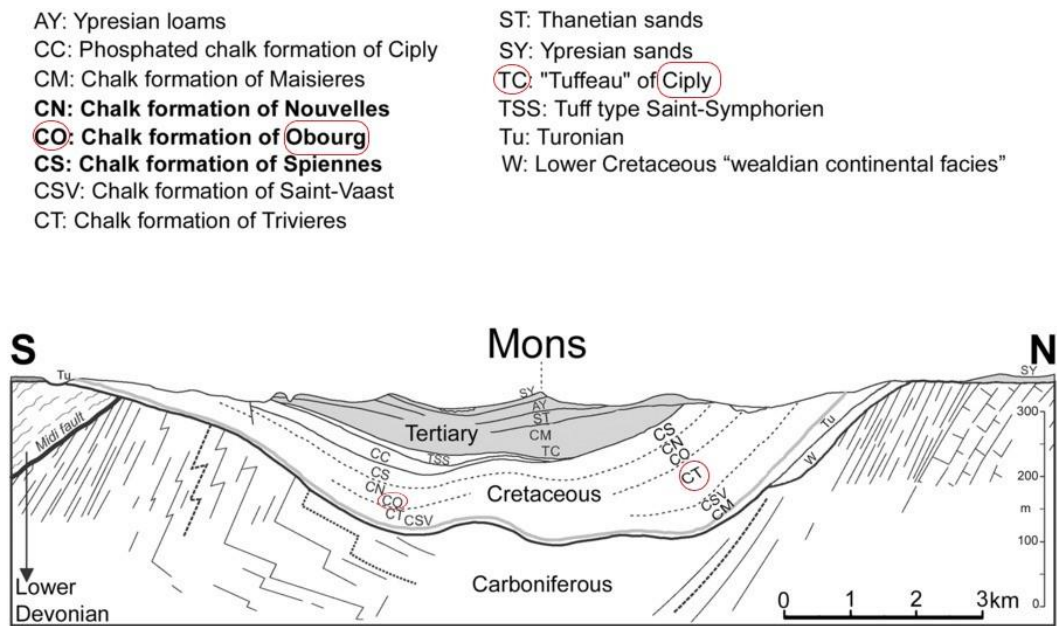


Figure 3- Transversal Schematic Profile of the Mons Basin, Showing the Different Cretaceous Chalk Formations[9]

Obourg Chalk, sometimes referred to as Mons Chalk, is a fine-grained white chalk, that crops out in the northern part of the Mons Basin. Furthermore, Obourg is a micritic chalk, which means it has mud-dominated texture. [9];[10];[11];[13]

It has a high porosity (an average of 43%), but a low permeability (an average of  $6.4 \times 10^{-16} \text{ m}^2$ ), which is typical of chalk. Pore radii of  $0.291 \mu\text{m}$  are also typical of this kind of chalk. [12]

Depending on the sample porosity, P-wave velocity varies between 2200 and 2700 m/s, whereas S-wave velocity ranges between 1400 and 1500 m/s. These Values were determined for dry samples.[12]

The Obourg Chalk samples were collected from a quarry located in Harmignies, and the Ciplly Chalk samples from an underground quarry in the same area called La Malogne. *Table 1* summarizes the main characteristics of both rocks.

Table 1- Obourg and Cibly Chalks' Characteristics[59]

	Obourg Chalk	Cibly Chalk
Mineralogical Composition	Calcite	Calcite, Fluorapatite
Grain Density (kg/m <sup>3</sup> )	2720	2730
Bulk Density (kg/m <sup>3</sup> )	1550	1680
Average Porosity	0.43	0.39
Average Permeability (m <sup>2</sup> )	6.4 x 10 <sup>-16</sup>	4.0 x 10 <sup>-14</sup>

Cibly Phosphatic Chalk has a more heterogeneous composition with not only calcite, which is the main component, but also fluorapatite and other minerals, which gives the rock a brownish color. In *Figure 1*, typical microstructure images obtained with SEM technique are shown for the two chalks. The SEM micrographs in *Figures 2b/2c* show the presence of high-density nodules, with a composition (obtained by DRX analysis) made of oxygen, calcium, carbon, phosphorus and fluorine, a chemical composition close to that of fluorapatite. In *Figure 2a*, we can clearly see a homogeneous matrix of small calcite minerals which makes up more than ninety-nine percent of this type of chalk. These brain-like nodules in *Figure 2c* can be attributed to the action of cyanobacteria which caused a cortex of this shape to be precipitated on the grains.[14]

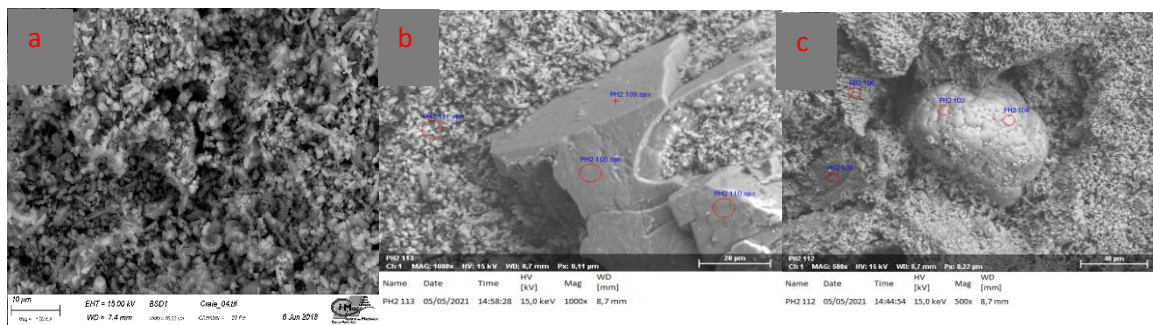


Figure 4- SEM Graphs on Chalks

**a-** SEM of Obourg **b-** Big Calcite particle in Cibly SEM **c-** Brain-like Nodule in Cibly SEM

As the heterogeneous texture of the Cibly Phosphatic Chalk is probably affecting its mechanical properties, the samples under study were systematically cored away from the nodule-rich areas using the CT scan density maps as a guide during the coring process. Note that despite the similar porosity

values (about 39% compared to 43%), the Cibly Phosphatic Chalk has a permeability which is two orders of magnitude higher than the Obourg Chalk as shown in *Table 1*.

In the following paragraphs, we will find the detailed description of the preparation procedure done in the process to get the ideal samples for the tests to be carried out.



*Figure 5- Cored Chalk Blocks*

The chalk blocks collected in the quarry were cored perpendicularly to the bedding to produce cylinders of 25 mm in diameter, they have been then cut and machined to transform them to the shape of a disk having a length ranging between 1 to 10 mm. Before continuing the preparation procedure, the samples were then left to dry in the oven at a temperature of 60° for at least 24 h to ensure the removal of any water from the cutting machines.



*Figure 6- Diamond Drill Coring Machine*

A petrophysical screening of porosity has been subsequently conducted with the aim of selecting a uniform group of samples and removing the outliers.

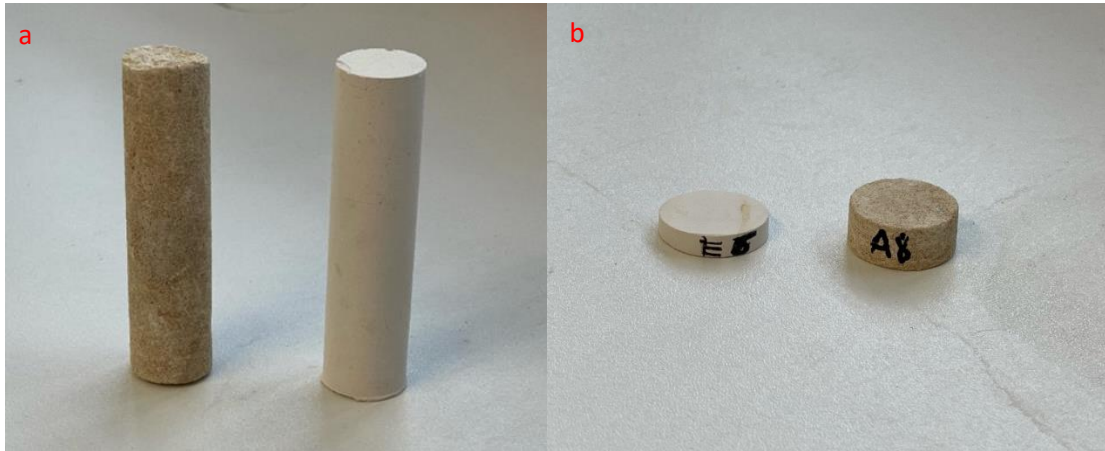


Figure 7- Chalk Sample Preparation

**a**- Cores of a 25 mm Diameter    **b**- Disks of length 1-10 mm

Dealing with un-saturated samples, the porosity has been computed using the grain and bulk density ( grain and bulk , respectively):

$$\phi = \frac{\rho_{Bulk}}{\rho_{Grain}} \quad (1)$$

With grain representing the density for pure calcite ( $2720 \text{ kg/m}^3$ ), confirmed by helium pycnometer on chalk grains. [12]

Taking into consideration that part of our testing procedure was going to be on contact angle measurements, we had a problem that needed to be tackled, which is the high absorption rate that comes with using such high porosity types of chalk.



Figure 8- Droplet Absorption

**a-** Water Drop has yet to Touch the Surface **b-** Absorption Initiated after the Drop Touches the Surface **c-** The Drop is Fully Absorbed

Figures 8a/8b/8c show us 3 different frames, all evidently taken within less than one second of the instant absorption process that occurs to a liquid droplet upon coming in contact with a sample of the high porosity chalks we are working with.

As a result, all attempts at studying the shape of any liquid droplet on the surface of our samples were deemed impossible with such preparation.

Therefore, the next step for us in the preparation procedure of our samples was an attempt to saturate them with a material that can eliminate the absorption problem and allow us to perform all the measurements we are looking for.

The Saturation process was fulfilled using an Epoxy Resin, namely EpoFix Resin by Struers.

The resin, after being prepared and mixed with the hardener, would be put in contact in excess amounts with the samples in order to penetrate as much as possible and fill up all the holes extinguishing the porosity, and thus eliminating the absorption effects.



Figure 9- EpoFix & Hardener

The saturation process basically consists of four steps:

- a) Putting the sample in a vacuum chamber to remove the air from the pores to enhance the penetration of the resin.
- b) Preparing the Resin/Hardener mixture.
- c) Dropping the resin all around the sample for penetration.
- d) Removing the excess hardened resin surrounding the samples.

### Vacuum Chamber

The vacuum chamber we are working with was assembled in the CYU GEC Geomechanics Laboratory by connecting a small box to a vacuum pump and leaving the samples inside for the vacuuming process for at least eight hours.



Figure 10- Vacuum Chamber

## Preparing the Mixture

There are ways to create a mixture with the right ratio between the the EpoFix Resin and EpoFix Hardener according to the previously set guidelines by the manufacturing company Struers.

It can be mixed based on:

Volume / Volume Ratio : 15 Resin / 2 Hardener

Mass / Mass Ratio : 25 Resin / 3 Hardener

Upon putting the required amounts of both liquids, a continuous mixing for two minutes is required in order for the 2 liquids to blend together properly, and from that moment, the hardening process will have been activated. Therefore, the saturation must be initiated as soon as possible in order to ensure that we have as much penetration as possible before the resin is completely hard and the propagation ceases through the sample pores.

## Dropping the Resin all around the Samples for Penetration

In order to maximize time efficiency, multiple samples are put together and exposed to the resin at the same time.

After the passing of this time interval, a small mechanical valve fixed with the conducting pipe to the freshly prepared resin mixture is open, and the negative pressure ( vacuum ) inside the box would create a suction force to pull the resin to the inside.

Upon the emptying of sufficient amount of the prepared resin, the pump is turned off, and the samples are left fully immersed in the resin over night to ensure that we have propagation in the pores to the utmost potential.

## Resin removal

After being left overnight, we open the box to find a hardened block of resin with the samples inside.



*Figure 11- A Resin Block Filled with Samples*

We take a block like that in *Figure 11* and start cutting to separate the different samples and remove all the excess resin from our saturated samples.

What we basically end up with is small disks of saturated chalk samples and these samples should be made sure that they do not have any small layers of resin on top as these layers could actually impact our measurements of the contact angle.

Thus, the next step of our procedure was to do some polishing using the Silicon Carbide papers going in a gradually increasing order of fineness from 120 to 240 to 4000 grits. The polishing process actually plays two parts in our case:

Removal of excess resin and eliminating doubts about whether or not a small layer of resin still remains on the surface of the samples to be studied.

Unifying surface conditions for all the samples to be measured in order to eliminate the effects that roughness could have on the contact angle measurements.

In order to be sure that what we are actually measuring is the contact angle on a saturated chalk sample and not on a small layer of pure resin, we attempted to use a numerical microscope to check if all the resin was removed.

During polishing, we can easily see the scratch marks on the resin from the silicon carbide papers, and thus these marks can be used as a reliable way to check if we still have a layer on the surface.

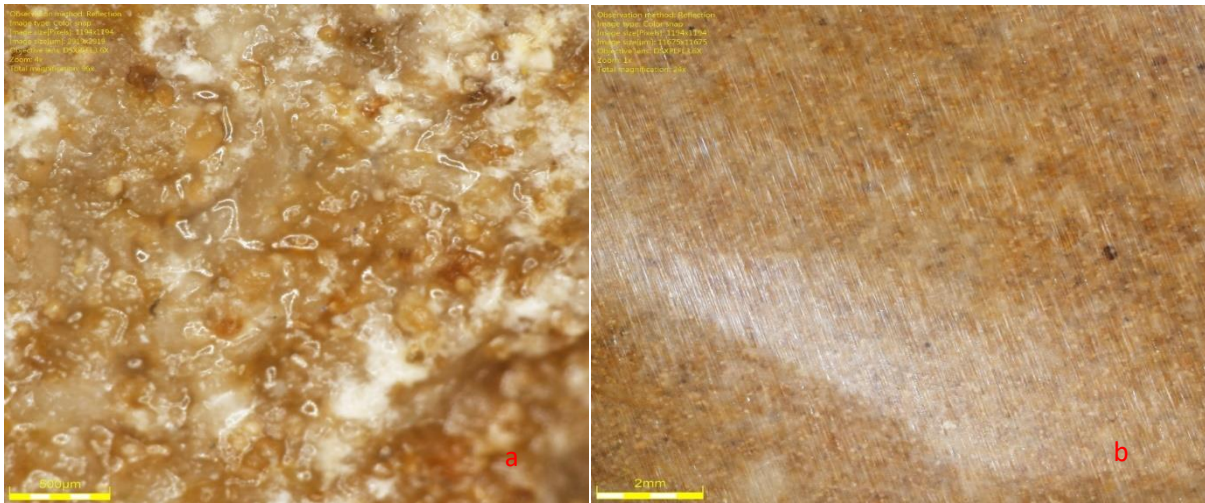


*Figure 12- Remaining Layer of Resin*

***a-** An Evident Unpolished Layer of Resin on the Surface   **b-** An Evident polished Layer of Resin on the Surface*

This can only mean that further polishing is required to remove this remaining layer on the surface that can only be seen using the microscope; however, with that lies another difficulty: Too much polishing might cause that we not only remove the resin layer, but also go too deep in the surface of the sample and accidentally arrive at a level where has not been sufficient penetration by the resin, like in *Figure 13*.



*Figure 13- Arrival at an Unsaturated Level within the Sample*

This has caused us to rethink about the credibility of our preparation procedure, because of the possibility that the values we received are due to a small unnoticed resin layer the surface, and to try to enhance it so as to be able to produce results that truly bring about the topic in study.

According to the levels of preparation previously obtained, we had the idea that maybe changing the saturating fluid would help divert us from this problem.

As a result, the idea was to choose another fluid capable of saturating the pores and solidifying on the inside to eliminate the effects of porosity on the contact angle measurements procedure.

Since information about water contact angles associated to different resins is not widely available, we decided to test multiple different resins to compare their values and check whether or not it is worth changing the type we are currently working with.

Therefore, we contacted Struers, the same manufacturing company that produces the EpoFix Resin, and inquired about different types of resins that they can offer.

Table 2- Different Resins Produced by Struers

Resin	Material	Curing time	Shrinkage	Application
 <b>EpoFix</b>	Epoxy	12 hours	*	For vacuum impregnation - low viscosity
 <b>ProntoFix</b>	Epoxy	90 min.*	*	For mounting and preparing specimens the same day
 <b>SpeciFix-40</b>	Epoxy	3.5 hours at 50 °C	*	Extremely good adhesion
 <b>CaldoFix-2</b>	Epoxy	1.5 hours at 75 °C	*	For all-round vacuum impregnation
 <b>LevoCit</b>	Acrylic	20 min.	**	Good edge-retention and planeness
 <b>VersoCit-2</b>	Acrylic	10 min.	****	For routine examination
 <b>DuroCit-3</b>	Acrylic	30 min.	*	Fast curing and no shrinkage
 <b>ClaroCit</b>	Acrylic	20 min.	***	For extraordinarily clear mounts
 <b>ViaFix</b>	Acrylic	20 min.	***	For vias and microvias

(\*) 1 is best

EpoFix being the Resin previously used, we decided according to the company’s recommendations to try the Specifix-40, CaldoFix-2, and the LevoCit. This group would also allow us to test the difference that using an acrylic, instead of epoxy, resin might have on the contact angle values that we shall obtain, as we thought that we might have a difference in wettability between these two materials.

However, the preparation for each resin can be completely different from one to one another. The main difference depends on the “ curing time ” as is evident in *Table 2*.



Figure 14- Prepared and Hardened Samples of CaldoFix-2, LevoCit, and SpeciFix-40 (From Left to Right)

During the preparation, of the SpeciFix-40 and the CaldoFix-2, it was required to admit the samples during the “ curing time ” in the oven, and this made us notice that the elevated heat allowed us to enhance greatly the propagation of the resin in the pores.

Table 3- Mean Value of Contact Angle Measurements on Different Resins

	LevoCit	SpeciFix-40	CaldoFix-2
Mean	80.73	87.29	74.59
SD	2.83	3.6	6.19

As we can see, the values are very close to those that we previously got with the EpoFix resin, and therefore we can infer that the tested resins do not demonstrate a difference in wettability, and thus in the measured contact angle values.

Despite the fact that the results from the different resins we tested did not prove helpful, the preparation procedure for them gave us an idea to try with the EpoFix.

So, we tried to put the EpoFix saturated samples in the oven, even without any previous vacuuming, and the results were even beyond our expectations.



Figure 15- Difference in Penetration between the Previous(Right side) and Final(Left side) Method of Preparation

Despite not putting the samples in the vacuum conditions, we had an incredible amount of penetration as is evident in *Figure 13*.

We can barely see a small line down the center, and this means we can easily polish the surface in way that we can ensure we no longer have a small layer at the surface, and still not have any worries about going too deep in the sample without worrying that we might reach an unsaturated part on the inside.

## 2.2. Advancing Angle Measurements

After having optimized the preparation to the utmost potential, we can finally proceed to the testing procedures.

Our process to get the surface energy of the chalk samples will mainly depend on Contact Angle Measurements.

These Measurements are done using a Sessile Drop Contact Angle Goniometer.

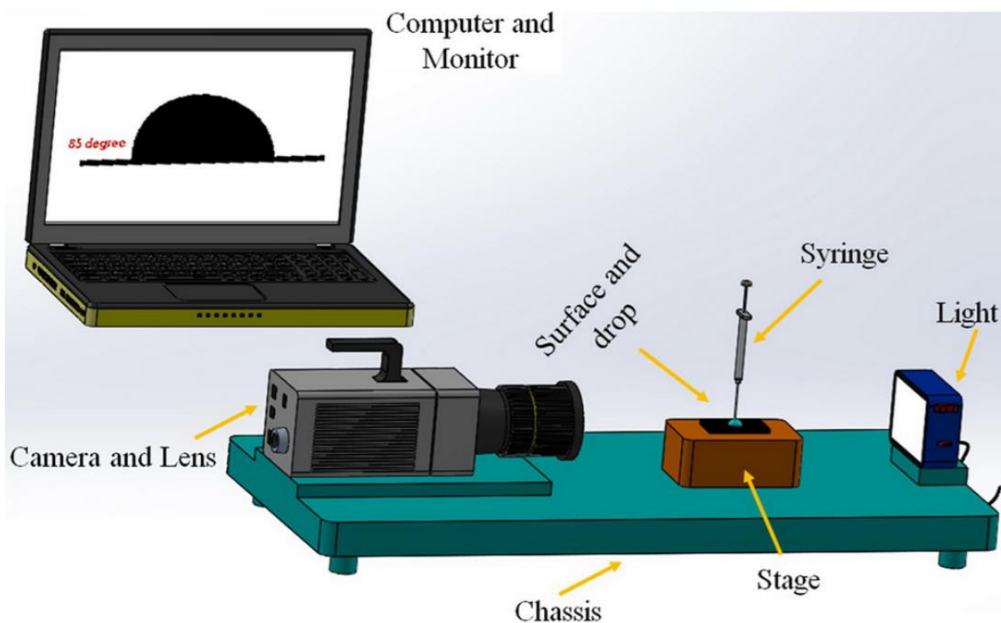


Figure 16- Goniometer Simplified Set Up

The Sample is put on the device, and then a sessile drop is placed on the surface of our sample; after that, we take a picture measuring the angle.

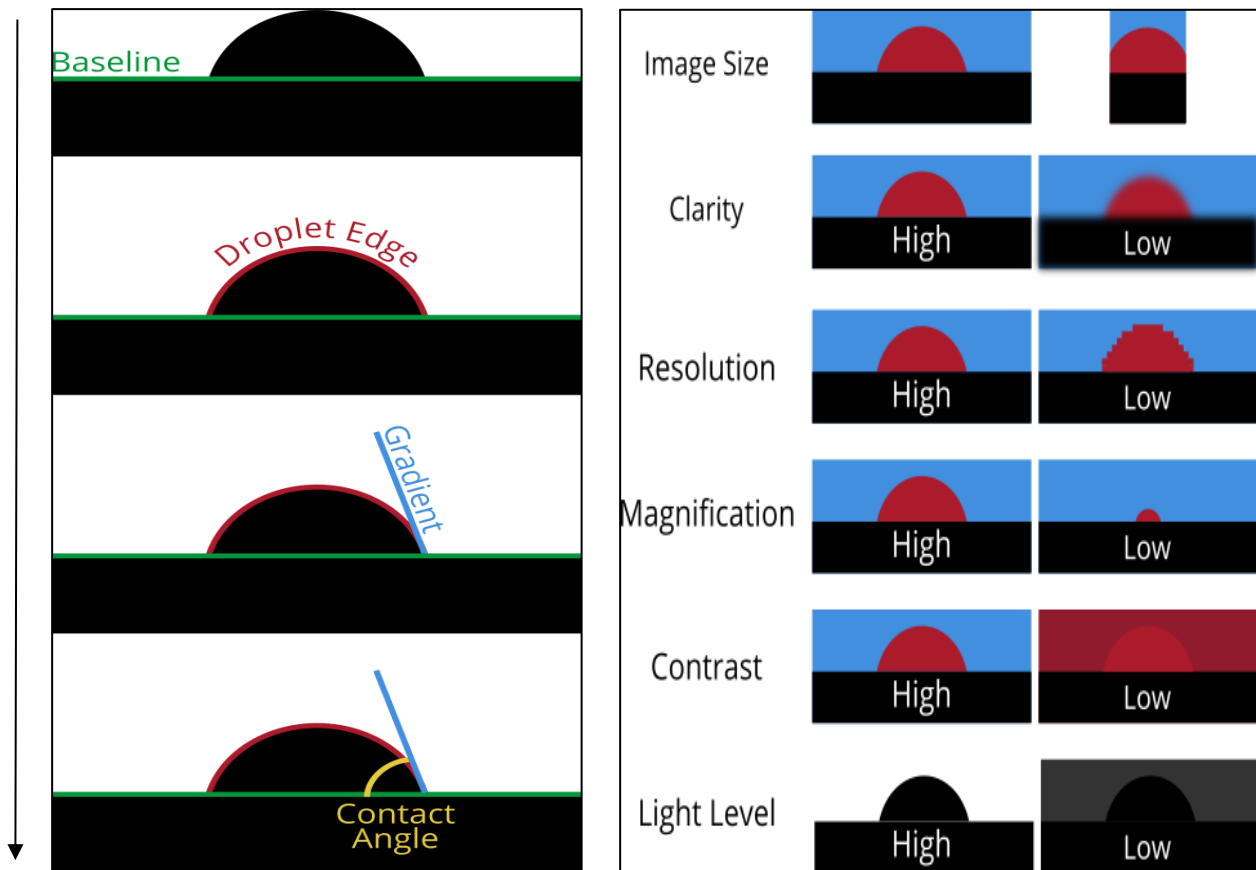


Figure 17- Measurement Procedures, and Variables Controlling the Quality of Measurements [15]

Where:

- **Image Size:** It is required that the entire droplet must be contained in the image.
- **Clarity:** A clear image of the droplet is required, as a ‘fuzzy’ image makes it more difficult to locate the edges, and thus to properly measure the contact angle.
- **Camera resolution:** The image must not be highly pixelated to clearly find the desired edges.
- **Magnification:** The more pixels covered in image (the larger the optical image is) , the higher its resolution will be.
- **Contrast:** Contrast is important for separating the droplet from its background and locating its edges.
- **Lighting:** It is necessary to clearly see the droplet; hence, we must avoid that the lighting is too light or too dark which might affect the contrast and background.
- **Depth of Field:** It is possible to alter the aperture of the lens of the camera to change the “ depth of field ”, which is an ‘area either side of the focal point which you consider to be in focus’. This could be done in case the entire depth our droplet is not in focus, which could affect the accuracy of our measurements. [15]

Furthermore, there are a few imperative factors to take into account when dealing with contact angle measurements, which include:[17]

- Roughness Factor

- Heterogeneity Factor

- Particle Shape Factor

- Particle Size Factor

The main two factors whose effects we focused on diminishing were the *Roughness*, and *Heterogeneity*.

- **Roughness:**

In order to assess the roughness factor on our samples, we decided to use the Confocal Laser Scanning Microscope ( CLSM ), which can quite easily give us accurate readings on our samples.

We had available for us the Zeiss LSM 980 model with Airyscan 2.



Figure 18- The CLSM

The CLSM is a light microscope that uses a laser beam to focus on a sample. It does so by using a set of mirrors that can move the beams very precisely. The objective lens is then focused on the sample, and the image is built up pixel-by-pixel by collecting the emitted photons from the fluorophores in the sample.[18]

This device can also detect the autofluorescence of different materials in the samples being tested and display them showcasing different frequencies.

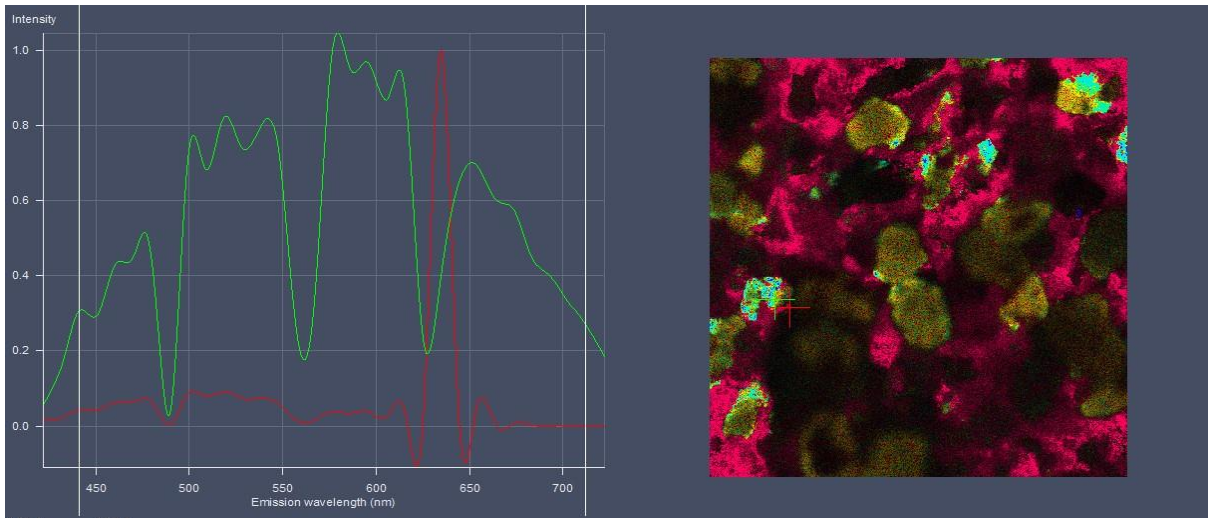


Figure 19- Autofluorescence of Different Materials in our Samples

And in our case, the roughness measurement was essential in order to make sure that our polishing process was up to the required standards.

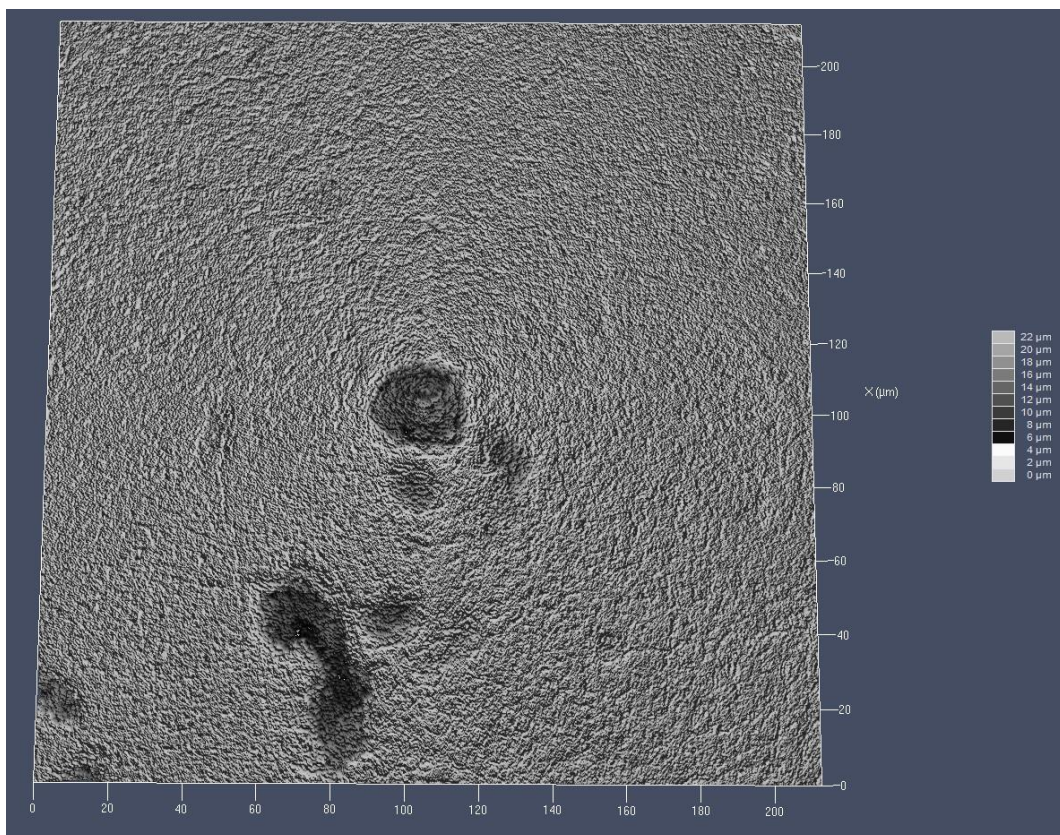


Figure 20- The CLSM Roughness Measurement

Figure 20 shows a clear view of the roughness of the surface.

This measurement bodes well with the values accepted for the Wenzel Equation:

$$\cos \theta_w = r \cos \theta \quad (2)$$

Where:

$\theta_w$  = Measured Contact Angle

$\theta_Y$  = Ideal ( Young ) Contact Angle, which assumes a perfectly smooth surface.

r = Roughness Ratio

The ideal contact angle actually depends on the “ideality” of the surface which must be smooth, flat, homogenous, inert, insoluble, nonreactive, non-porous, and of non-deformable quality. These conditions are almost never met by real surfaces.[17]

The Roughness Ratio is defined as the ratio between the actual and projected solid surface area ( $r=1$  for a smooth surface and  $> 1$  for a rough surface).

Wenzel equation applies, if the drop is larger than the roughness scale by two to three orders of magnitude, which applies to our case where we have such low values of roughness and where our droplets were of the order of mm or  $10^{-1}$  x mm.[19]

#### - Heterogeneity:

In our case, we can consider the heterogeneity only as a cause of the resin saturation procedure, and disregard impurities in our rock samples as studies have shown that this type of chalk from the Mons Basin in Belgium has an impurity percentage of less than 0.1 %.

To deal with this matter, we used the Cassie-Baxter equation:

$$\cos \theta_C = x_1 \cos \theta_1 + x_2 \cos \theta_2 \quad (3)$$

Where:

$x_1$  = Surface Fraction of Material 1

$x_2$  = Surface Fraction of Material 2

$\theta_1$  = Contact Angle with Material 1

$\theta_2$  = Contact Angle with Material 2

$\theta_C$  = Contact Angle with the Saturated Specimen

Where all the angles in the equation are relevant for a specific fluid – surface interface and would change if the fluid changed.

In our case, we have the  $\theta_C$  as the measured contact angle, the  $x_1$  being the surface fraction of chalk which we assumed to be given by and equal to the porosity, the  $x_2$  as  $(1 - x_1)$ , and  $\theta_1$  as the contact angle between the liquid and the saturating resin that we had measured also using the goniometer.

This leaves us with only one unknown which is  $\theta_2$ , the contact angle between the sample liquids we are using and the chalk component of our saturated samples.

There are two modes in which the contact angle can be measured:

### Static Contact Angle Measurement:

It is imperative to follow the guidelines showcased in *Figure 17*, as they ensure that the measurements performed give a correct reading of the **STATIC** contact angle.

Procedure must be finished as soon as possible in order to avoid any evaporation effects; in addition to the need to be very delicate in order not to have any displacement effects on the droplet on the surface to get an accurate **STATIC** reading.

## Dynamic Contact Angle Measurement:

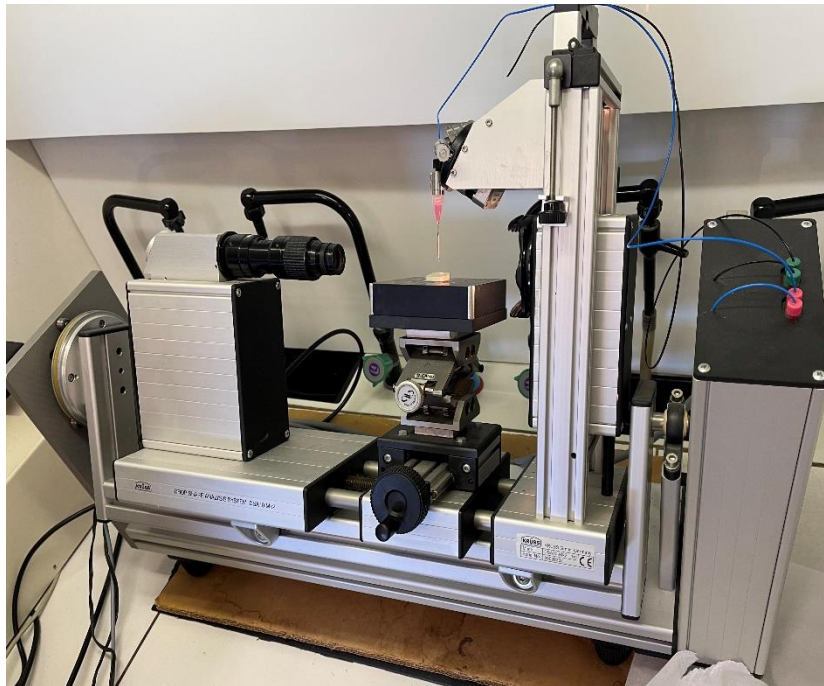


Figure 21- Dynamic Contact Angle Measurement

The main difference between these two types of measurements is the fact that for the Dynamic Measurement, the goniometer is put in motion, in which it is set to be rotated by a *tilting* angle which could even go up to a full ninety degrees. This would allow the drop to glide on the surface of our sample.

In our case, we are waiting for the exact moment that the drop is no longer restricted by the constraints of wettability and friction (due to the surface roughness), and finally starts to glide on the surface. At that moment, we repeat the procedure mentioned in *Figure 17* to obtain two angles on both sides of the drop, an ***Advancing*** angle on the side corresponding to the gliding direction, and a ***Receding*** angle on the opposite side.

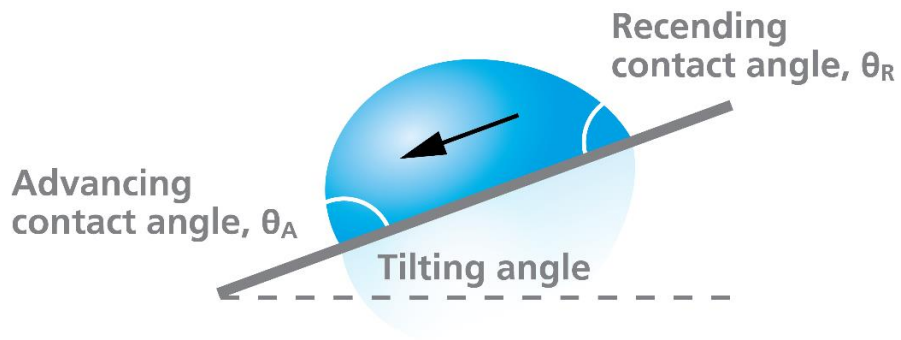


Figure 22- Dynamic Contact Angles[16]

In our case, all contact angles used in our calculation were actually advancing contact angles obtained by doing dynamic measurements, this includes all the  $\theta_1$  angles between our sample liquids and pure resin samples, and all the  $\theta_C$  angles measured on the saturated samples.



Figure 23- A Few Resin and Saturated Rock Samples

### 2.3. O.W.R.K Model

The Owens, Wendt, Rabel and Kaelble ( O.W.R.K ) Model is a standard model used for calculating the surface free energy of a solid based on the contact angle with several liquids by dividing the surface free energy into a polar part and a disperse part.[20]

However to get there, a long road was passed starting with the Young's Equation, which can be considered as the basis of all SFE theories:

$$\gamma_{sv} = \gamma_{sl} + \gamma_{lv} \cos \theta_Y \quad (4)$$

Where:

$\gamma_{sv}$  = Surface Free Energy of the Solid

$\gamma_{sl}$  = Interfacial Tension Between the Liquid and Solid

$\gamma_{lv}$  = Surface Tension of the Liquid

$\theta_Y$  = Contact Angle

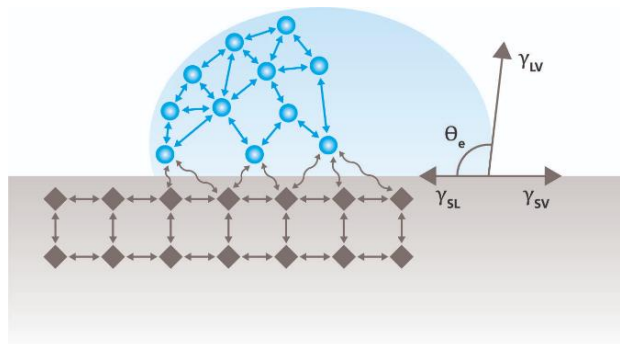


Figure 24- Components of the Young's Equation[21]

The problem with Young's is that it requires a very complicated measurement or calculation of the interfacial tension between the liquid and the solid under study.

Many tried to formulate the solid-liquid interactions, mainly Fowkes, who divided the interaction into different components by assuming that that  $\gamma_{sl}$  is determined by various interfacial interactions that depend on both, the properties of the measured substrate and those of the measurement liquid. Fowkes

assumed that the surface free energy of a solid (and surface tension of a liquid) can be divided into independent components, associated with specific interactions:[21]

$$\gamma_{sv} = \gamma_{sv}^d + \gamma_{sv}^p + \gamma_{sv}^h + \gamma_{sv}^i + \gamma_{sv}^{ab} + \gamma_{sv}^o \quad (5)$$

Where:

$\gamma_{sv}^d$ = Dispersion Component

$\gamma_{sv}^p$ = Polar Component

$\gamma_{sv}^h$ = Hydrogen Component

$\gamma_{sv}^i$ = Induction Component

$\gamma_{sv}^{ab}$ = Acid-Base Component

$\gamma_{sv}^o$ = All Other Remaining Components

Furthermore, Good and Girifalco came up with an interesting equation:[22]

$$\gamma_{1,2} = \frac{1}{2} (\gamma_1 + \gamma_2 - \gamma_1 \gamma_2 \phi)^{1/2} \quad (6)$$

Where:

$\gamma_{1,2}$  = Interfacial Tension Between Materials 1 and 2

$\gamma_1$  = Surface Energy of Material 1

$\gamma_2$  = Surface Energy of Material 2

$\phi$  = Interfacial Interaction Parameter

Owen and Wendt continued the Fowkes idea; however, they stated that all components in the right side of the equation, except  $\gamma_{sv}^d$ , can be considered polar ( $\gamma_{sv}^p$ ). Then they combined it with the Good Girifalco definition of the interfacial tension assuming  $\phi = 1$  to get:

$$\gamma = \gamma^d + \gamma^p \tag{7}$$

And Then:

$$\gamma_{sl} = \gamma_{sv} + \gamma_{lv} - 2\sqrt{\gamma_{sv}^d \gamma_{lv}^d} - 2\sqrt{\gamma_{sv}^p \gamma_{lv}^p} \tag{8}$$

To satisfy eq. (8), we need at least two sample liquids with available disperse and polar components of the surface tension including that at least of the two liquids must have a polar component.

According to the two-component model, the interfacial tension depends on the possibility of the polar and disperse components to form interactions with corresponding parts of the adjacent phase.

Assigning the orange color to represent the dispersive component, and the dark blue to the polar component, the following diagram symbolizes the different interactions by means of hands, whereby only "matching" hands can link with one another:[20]

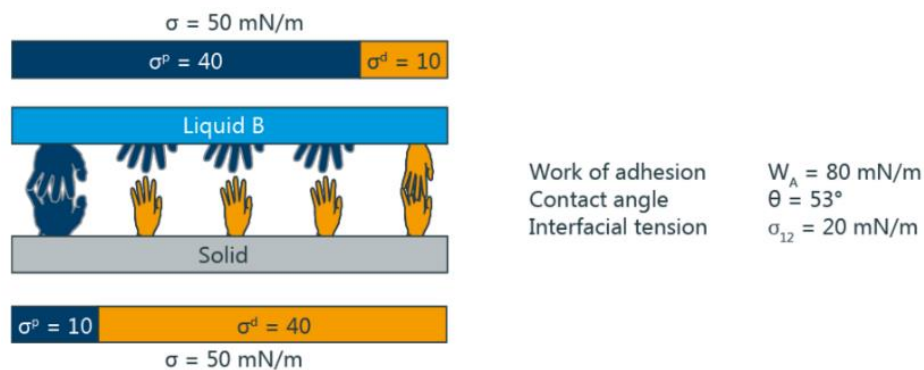


Figure 25- Schematic Representation of the Two-Component Phase Contact Mode without Compatibility

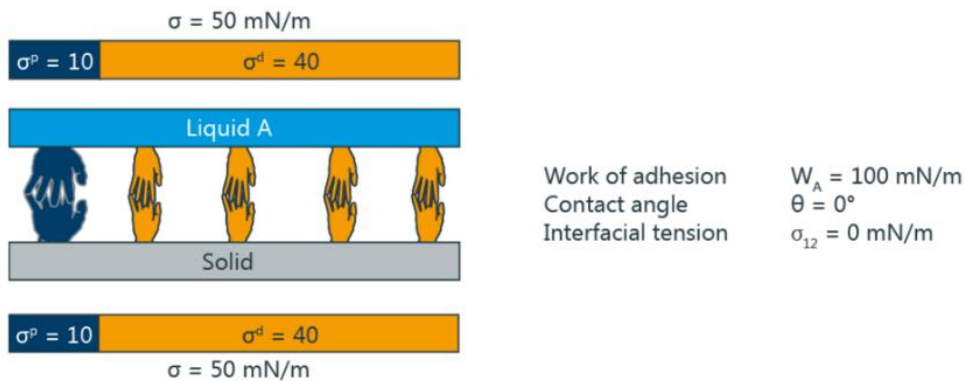


Figure 26- Schematic Representation of the Two-Component Phase Contact Mode with Compatibility

And finally, to reach the final formula of the OWRK Model, we combine *eq. (8)* with the Young's Equation (*eq. (4)*) to get:

$$\sqrt{\gamma_{sv}^d \gamma_{lv}^d} - 2\sqrt{\gamma_{sv}^p \gamma_{lv}^p} = 0.5\gamma_{lv}(1 + \cos \theta_Y) \quad (9)$$

The most important assumptions made in the O.W.R.K model are:

The liquid is pure.

The solid is smooth and chemically homogenous.

There are no chemical reactions between the liquid and the solid.

No real system will completely satisfy all of these assumptions; however, the O.W.R.K Model is very widely viewed as one of the most reliable ways to calculate the SFE. [23]

Applying the model would require a rearrangement of *eq. (8)* to get an equation of a straight line:

$$\frac{\gamma_{lv} \cos \theta_Y}{2\sqrt{\gamma_{lv}^d}} - \frac{1}{\left(\sqrt{\gamma_{sv}^p}\right) \frac{\sqrt{\gamma_{lv}^p}}{\sqrt{\gamma_{lv}^d}}} = \sqrt{\gamma_{sv}^d} \quad (10)$$

Having  $\frac{\sqrt{\gamma_{lv}^p}}{\sqrt{\gamma_{lv}^d}}$  and  $\frac{\gamma_{lv} \cos \theta_Y}{2\sqrt{\gamma_{lv}^d}}$ , we can simply find the  $\sqrt{\gamma_{sv}^p}$  as the slope of the line

and infer  $\gamma_{sv}^p$  from it, as well as get  $\sqrt{\gamma_{sv}^d}$  and deduce  $\gamma_{sv}^d$  from it.

The data required to input into the *eq. (10)* depends mainly on the Sample Liquids we choose to perform our contact angle measurements with.

In our case, we attempted to work five different sample liquids (with a purity that is higher than 99%) in an attempt to have as much diversity in dispersion/polarity components as possible and monitor their different effects on our samples and on the SFE calculation.

Each Sample Liquid will give us a point to input in the equation due to its *Polar* and *Dispersive* properties, and due to the contact angle that it forms with our samples and with the pure resin samples , thus enhancing the accuracy and reliability of our model.

We worked with Deionized Ultra-Pure Water, Diiodomethane (DIO), Formamide (FORMA), Dimethyl Sulfoxide (DMSO), and Glycerol (GLYC) Having the following Properties:

Table 4- Sample Liquids' Properties[25]

	WATER	DIO	FORMA	DMSO	GLYC
DISP $\gamma^d$	21.8	48.5	39.5	36	34
POL $\gamma^p$	51	2.3	18.7	8	30
TOT $\gamma$	72.8	50.8	58.2	44	64

This allowed us to work with three highly *Dispersive* liquids (DIO - FORMA - DMSO), one highly *Polar* liquid (WATER), and one having an almost equal amount of both components (GLYC).

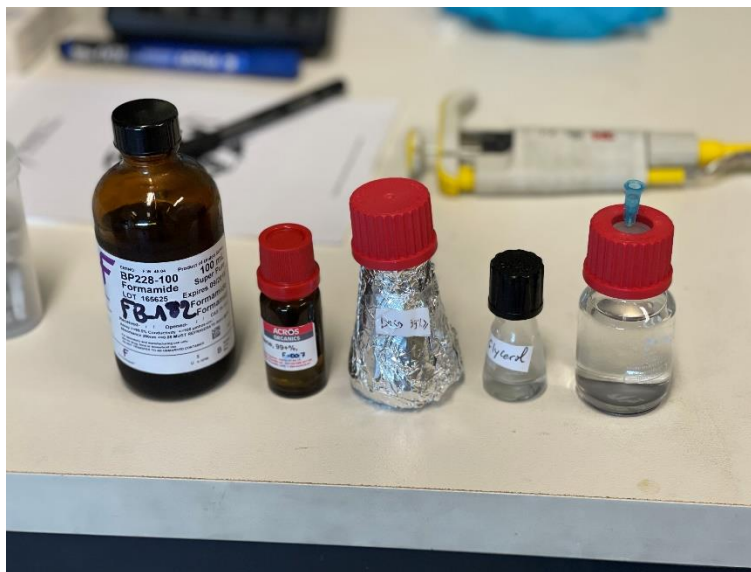
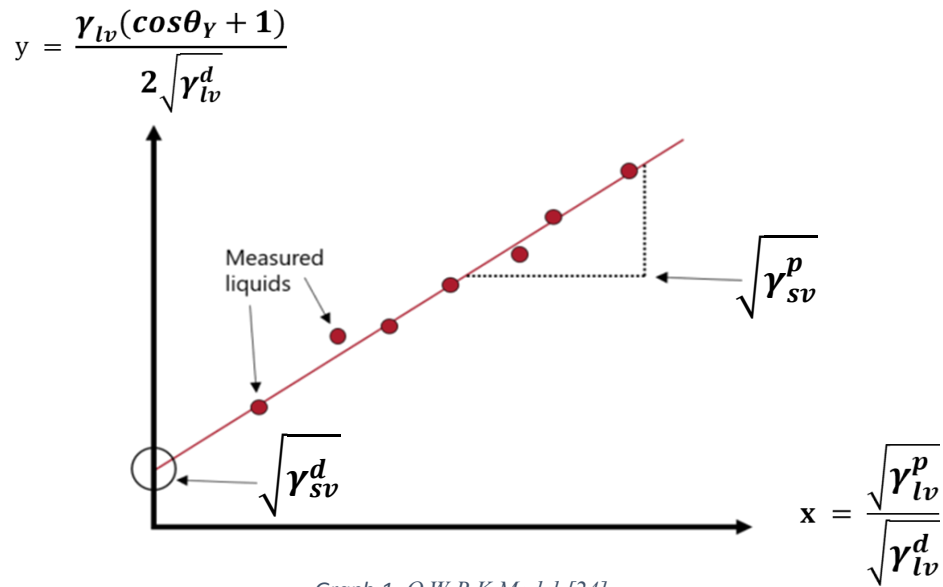


Figure 27- Sample Liquids: Formamide - Diiodomethane - DMSO - Glycerol - Ultra-Pure Water (Left to Right)

The measurements done with each liquid will allow us to have one point, which means that our case will consist of five points thus decreasing the error and enhancing the best fit of our straight line from which we will deduce the components of the SFE.



Graph 1- O.W.R.K Model [24]

After obtaining the values of both the Dispersive and the Polar components of our samples, we simply input the data into eq. (7) to get the SFE.

## 2.4. O.W.R.K Model with Calcites

Knowing that the main components of the Obourg and Ciply chinks are the calcite minerals, we decided that the next step in order to validate and getting a deeper understanding of the results is to reproduce the same procedure-which we previously performed on our chalk samples- on pure calcite minerals.

Nonetheless, there is a huge difference between these two cases, which is that when working with pure minerals, we are actually working with a solid sample that is not porous; this means that we no longer need to saturate with resin and then work on removing the effects using the Cassie-Baxter equation (*eq. (3)*).

To perform this procedure, we worked on two different Calcite samples and used three Sample liquids which are the Formamide, Diiodomethane, and the Deionized Ultra-Pure Water.

Albeit having a different origin of formation, we assume that the values that we will obtain from testing on the pure calcites, which are mainly found in sedimentary environments, and their metamorphized products, can be representative enough of the calcite particles constituting our chalk samples, which is mainly formed of the fossilized skeletons of coccolithophore phytoplanktons.[26],[27]



*Figure 28a- A Translucent Calcite*



*Figure 28b- A Translucent Calcite*

As we can see in *Figure 28a/28b*, there is another major and clear difference between these calcites and our previously prepared saturated chalk samples, which is the roughness of the surface on which we performed the Contact Angle measurements required to fulfil the O.W.R.K Model.

As a result, we performed some Measurements using the CLSM to identify the surface roughness values of these samples and try to see whether or not it is within the acceptable margins.

## 2.5. SCB & Fracture Toughness

A Surface Energy, the Fracture Energy, can also be identified using a number of other different methods which can be mechanical as well. Mainly the idea is to initiate a crack propagation in a specifically prepared sample in order to find the surface energy, either directly or indirectly.

Multiple set-ups can be prepared such as the Double Torsion Testing (DTT) used to calculate the fracture energy through the energy release rate based on the crack velocity according to the set-up:

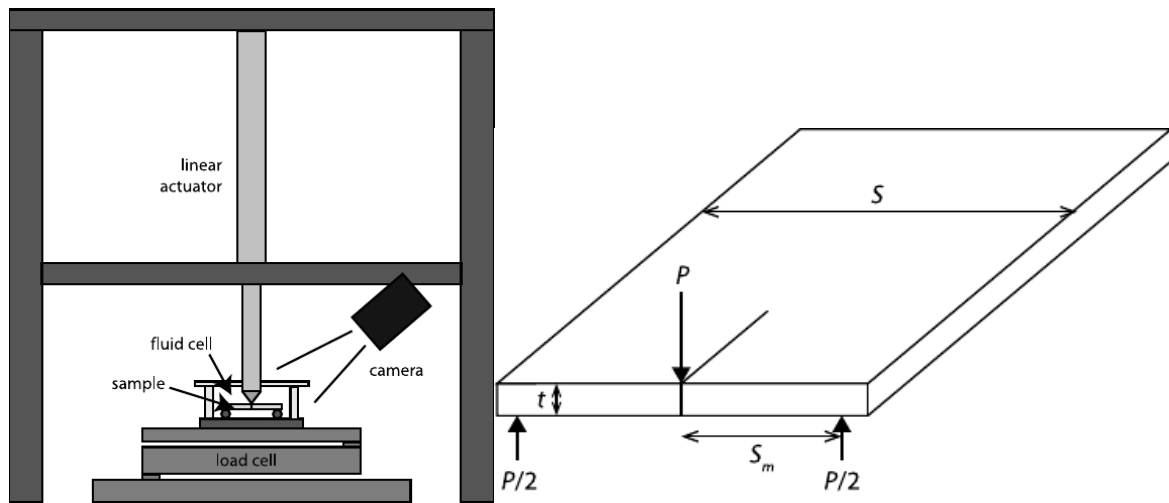


Figure 29- DTT Set-up[28]

And the calculations would be based off equations:[29]

$$\gamma_s^e = g_0/2 \quad (11)$$

Where:

$$g = \frac{3P^2 S_m^2}{2GSt^4 \psi} \quad (12)$$

Where  $g$  is the energy release rate,  $P$  is the applied load,  $S_m$  is half the distance between the supports,  $S$  and  $t$  are sample width and thickness,  $\psi = 1 - 0.6302\tau + 1.20\tau \exp(-\pi/\tau)$  is a geometric correction factor with  $\tau = 2t/S$ , and  $G$  is the Young's Modulus.

Which is dependent on:

$$v = \frac{-P_i}{P} a_i \frac{D}{B} \frac{dP}{dt} \quad (13)$$

Where  $v$  is the crack velocity,  $P_i$  and  $a_i$  are instantaneous measurements of load and crack length, and  $B$  and  $D$  are scaling constants.

Another way to calculate the fracture energy is by identifying the Fracture Toughness of our samples instead of the Energy Release Rate.

We can calculate the Fracture Toughness ( $K_{Ic}$ ) using multiple set-ups including the Semi-Circular Bend sample preparation and the Cracked Chevron-notched Brazilian Disk (CCNBD) preparation.

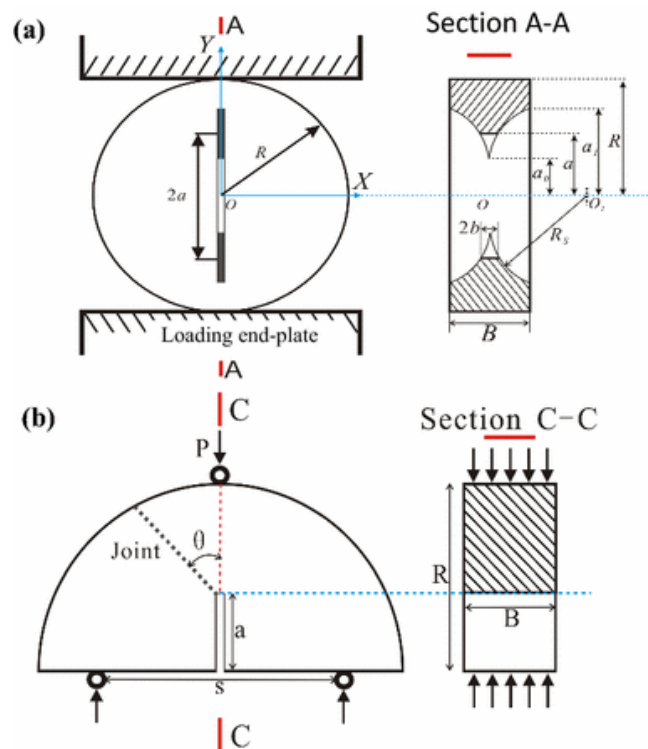


Figure 30- Crack Propagation Tests

- CCNBD - SCB [30]

The mode I stress intensity factor, also known as the fracture toughness, ( $K_{Ic}$ ) at the machined crack tips was computed by:[31-35]

$$K_{Ic} = \frac{F_{ax}}{B\sqrt{R}} Y^* \quad (14)$$

Where  $F_{ax}$  is the axial force applied on the CCNBD sample,  $B$  and  $R$  are the sample thickness and radius, respectively.

For the geometry used:

$$Y^* = u \exp(v \alpha_1) \quad (15)$$

Where  $u$  and  $v$  are constants listed in the ISRM norms and  $\alpha_1$  is the long half machined crack length normalized by the sample radius.

In our case, we were able to recreate the SCB procedure at the Geosciences Laboratory in CYU by attaching a special set-up to the available hydraulic press.

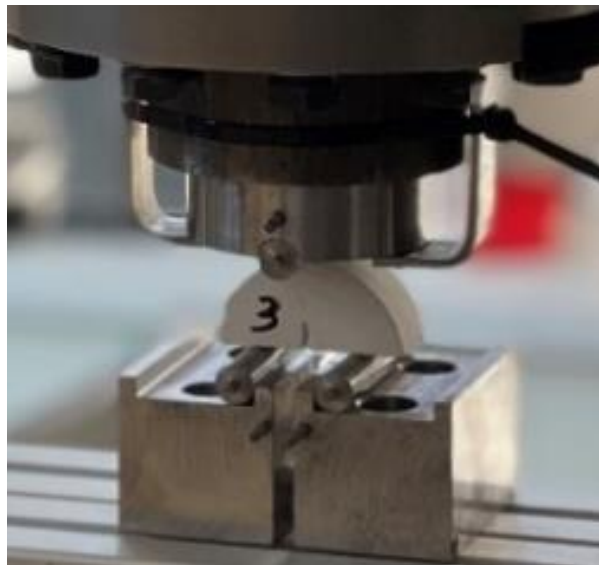


*Figure 31- SCB Set-up*

Our samples were prepared by preparing cylindrical cores with an internal diameter of 4.9 centimeters. These cores were then cut into smaller disks of a thickness of about two and a half centimeters and then cut in half to create the semi-cylindrical geometry.



*Figure 32- Creating the Notch with a Saw*

The notch was then prepared by using a hand saw having a thickness of one millimeter.

Nonetheless, all the samples were then checked one by one for the accuracy of preparation, and the values were all recorded since the thickness, the radius and the even the removed material play an important role as parameters affecting the mode I Intensity Factor value.

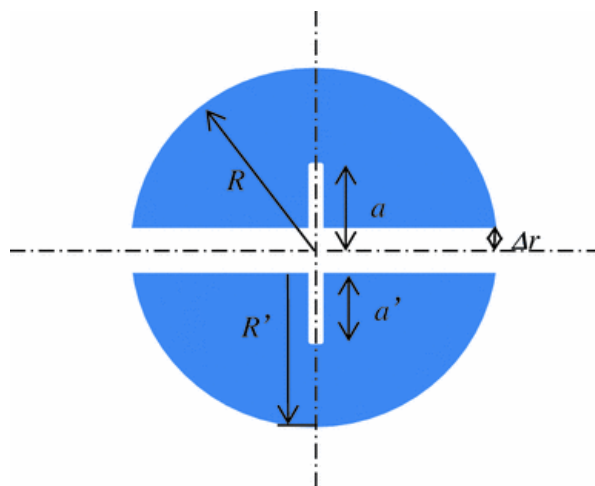


*Figure 33- SCB Geometry Parameters*

Where:

Table 5- Recommended Geometrical Dimensions of SCB Specimen[28]

Descriptions	Values or Range
<b>Diameter (D)</b>	Larger of 109 grain size or 76 mm
<b>Thickness (B)</b>	Larger of 0.4D or 30 mm
<b>Notch Length (a)</b>	$0.4 \leq \frac{a}{R} (= \beta) \leq 0.6$
<b>Span Length (s)</b>	$0.5 \leq \frac{s}{2R} \leq 0.8$

All these values will be used in the following equations:[36]

$$K_{Ic} = \frac{P_{max}\sqrt{\pi a}}{2RB} Y' \quad (16)$$

Where:

$$Y' = -1.297 + 9.516 \left( \frac{s}{2R} \right) - \left( 0.47 + 16.457 \left( \frac{s}{2R} \right) \right) \beta + 1.071 + 34.401 \left( \frac{s}{2R} \right) Y'^2 \quad (17)$$

Where a and R are the notch length and the radius of the sample respectively, in which their values represent the true radius and notch length, (taking into consideration the change due to the lost material that occurred while preparing the specimen)  $\beta = a/R$ ,  $P_{max}$  is the maximum load before failure, B is the thickness of the sample, and s is the spacing between the two lower points of load application.

These conditions meant that we aimed at working with specimen having the following specifications:

$$D = 4.9 \text{ cm}$$

$$B = 2.5 \text{ cm}$$

$$R = 2.45 \text{ cm}$$

$$s = 2.45 \text{ cm } ( s/2R = 0.5 )$$

$$a = 1 \text{ cm } ( \beta = 0.4 )$$

In order to enhance our notch preparation technique, we used a different machine equipped with a rotating belt whose edges are aligned with powdered diamond which would help the Grinding and cutting of any rock sample, and increase the precision and lower the thickness of the notch:



Figure 34- Precise Cutting Machine

However, we still performed measurements at each step in the preparation process and even after performing the test to make sure we input the true values into the equations which would ensure getting the most accurate Mode I fracture toughness values and eventually the Surface Fracture Energy values according to the following equation:

$$G_c = \frac{K_{Ic}^2 (1-\nu^2)}{E} + 2\gamma \quad (18)$$

Where  $G_c$  is the fracture energy,  $\nu$  is the poisson ratio,  $E$  is Young's Modulus, and  $\gamma$  is the Surface-Free Energy.

Note that *eq. (18)* is valid for plane strain conditions; in case of plane strain conditions, we can use :

$$\gamma = \frac{K_{IC}^2}{2E} \quad (19)$$

These tests were performed on both the Obourg and the Ciply chinks, in both dry and saturated conditions. The aim is to calculate the Fracture Energy of both types of rocks in dry conditions and then compare the effects of saturation on the mechanical properties of these samples.

For the Obourg chalk, we already had priori information on the Young's Modulus in both dry conditions, and in saturated conditions with different liquids including Deionized Water, Sodium Chloride (NaCl), Magnesium Chloride (MgCl<sub>2</sub>), Calcium Chloride (CaCl<sub>2</sub>) at different concentrations.

For the Ciply chalk, we needed to calculate the Young's Modulus in both dry and saturated conditions; thus, we performed some Uniaxial Compression Tests (UCT) in order calculate these values.

These tests required the preparation of samples in a different way, which is specific to be able to perform the UCT in the right way.

For this type of test, we need cylindrical samples where the length of the sample is twice the diameter; therefore, we decided to do some cores having an internal diameter of about twenty-five millimeters and then reduce the length from both sides to only fifty millimeters.

By making cuts on both sides of the cylinder, we are trying to make sure we have a flat surface that would not affect the credibility of the values obtained from the UCT. Nonetheless, when found to be necessary, further polishing was performed in order to ensure a flat surface, and then the new values for the length and mass of the cores were measured to consider any parameter alteration.

The sample is then placed between the two pistons of the hydraulic press, and the axial stress is increased according to a constant displacement rate of  $5 \times 10^{-4}$  mm/s, which corresponds to a strain rate of  $\dot{\epsilon}_{ax} \approx 10^{-6}$  s<sup>-1</sup>. These experiments were stopped after witnessing a macroscopic failure. Kindly note that this method follows the International Society for Rock Mechanics (ISRM) guidelines.[38]



*Figure 35- UCT with Evident Failure*

For the saturated conditions, we only obtained the data for samples saturated with Deionized Water.

The saturation was performed using the following set-up:



*Figure 36- Saturation Process*

The left side consists of a pump that helps remove the air from the big circular container, creating a Vacuum which remains constant at “-1” Bar. This helps remove the air from the pores in the samples thus enhancing the saturation process. The right side consists of a flask with the prepared solution connected both to a pump from one side, and to that same circular container. The pipe connecting the flask to the container is made so that after a long session in the Vacuum (usually at least 8 hours), the valve between them is opened and the solution will be sucked into the big container due to the negative pressure. The pump which is connected to the flask plays the role of de-airing the solution which will also enhance the overall efficiency of the saturation process.

In order to make sure that our samples, and our saturation process are acceptable, we performed some porosity measurements based on the following equation:

$$\emptyset = \frac{m_{Sat} - m_{Dry}}{m_{Sat} - m_{Imm}} \quad (20)$$

Where  $m_{Sat}$  is the saturated mass,  $m_{Dry}$  is the dry mass, and  $m_{Imm}$  is the immersed mass.

The immersed mass was measured by suspending the saturated sample in the flask filled with same solution with which it was saturated and then the mass was measured as per the following set-up:

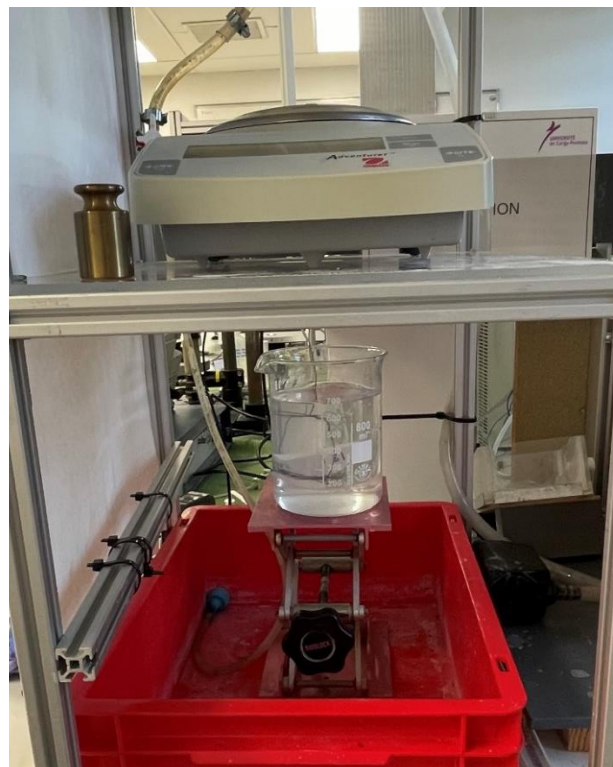
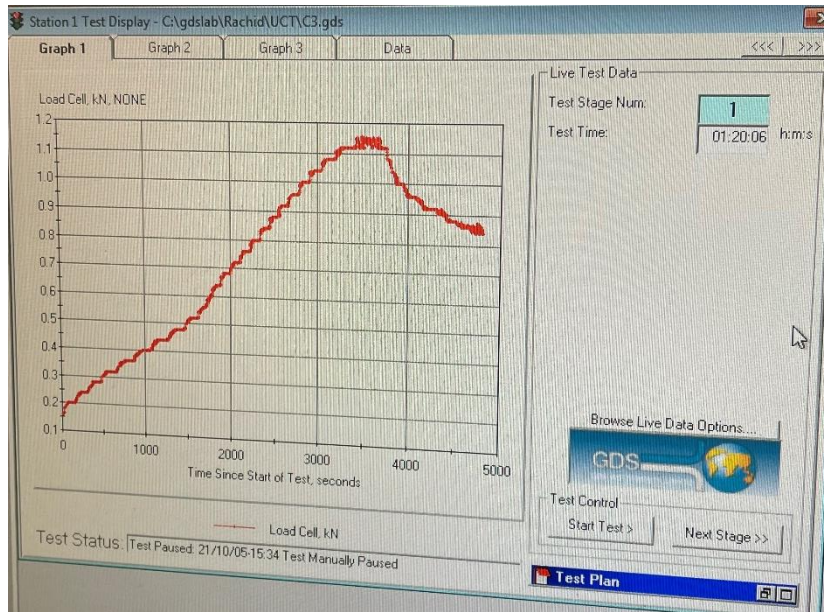


*Figure 37- Immersed Mass Measurement*

After performing these procedures, we could deduce the Young's Modulus of the Ciply chalk for both Dry and Saturated Conditions based of the data we accumulated while performing the Uniaxial Compression Test.



Graph 2- UCT

Graph 2 shows us a Load Vs Time which can be transferred into a Load Vs Displacement (since we have a constant displacement rate). Then, we change it to a Stress Vs Strain graph based off the two simple following equations:

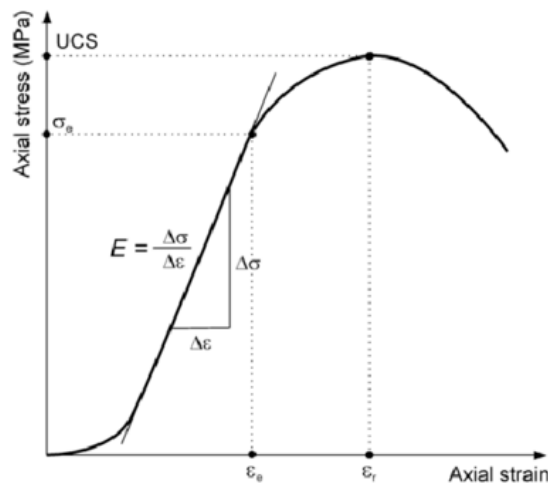
$$\sigma = \frac{F}{A} \quad (21)$$

and

$$\epsilon = \frac{\Delta L}{L_0} \quad (22)$$

Where  $\sigma$  is the stress, F is the Load applied, A is the surface area on which the load is applied,  $\epsilon$  is the strain,  $\Delta L$  is the Axial Displacement, and  $L_0$  is the initial Length of the specimen.

After transforming the data, we should have a graph similar to the following:



Graph 3- Stress Vs Strain

All that is left at this point is finding the slope of the straight part of the graph to find the Young's Modulus E just like in *Graph 2*.

After obtaining the Young's Modulus of the Ciply Chalk, we now have the necessary data in order to find the Fracture Energy of our samples from the SCB testing.

## 2.6. Brine Contact Angle Measurements on Calcites

After witnessing the effect of the different brines on the Fracture Surface Energy and on the mechanical properties, we wanted also to check how the presence of these ions might affect our surface properties. So, our next idea was to try and check how the wettability would change while using brines of different concentrations (and ionic strengths) by doing some Static Contact Angle measurements.

*Table 6- Salinity of the Used Brines*

Brines	Salinity (mol/L)
NaCl	0.075
	0.15
	0.3
	0.45
	1.05
MgCl <sub>2</sub>	0.04
	0.08
	0.16
	0.24
	0.57

The measurements were performed on the same calcites on which the O.W.R.K Model was applied. The Static Contact Angle measurement was used in this case instead of the Dynamic one due to the fact that our goal in this case was simply to identify a pattern and get a qualitative result which would increase our understanding of the situation. Performing a quantitative result leading eventually to the Surface Free Energy values in this case was not possible due to the absence of information regarding the Polar and Dispersive components of the used brines.

These measurements were consistently performed for each solution on the same set places in order to ensure that the difference in the results would be solely due to the difference in the interaction between the surface of our calcites and the solutions we were using.

## 2.7. SFE With AFM

Another way to determine the Surface Free Energy is using the Atomic Force Microscope.

The AFM can be used in multiple modes depending on the field, and the characteristic to be studied for which it is used and depending also on the material on which the testing is carried out.



Figure 38- AFM

The AFM that we used was the **Dimension Icon Atomic Force Microscope with ScanAsyst** by **Bruker**, which is a next-generation measurement system that brings new levels of performance, functionality, and accessibility to nanoscale researchers.[40]

In general, AFMs can be used in three primary modes:[41]

**Contact Mode:** Which is the original AFM and is the basis for all techniques where the probe tip is in constant contact with the sample. In this case, the tip connected to the cantilever of the AFM scans along the surface whose topography induces a vertical deflection of the cantilever which will be used to reconstruct an image of the topography.[42]

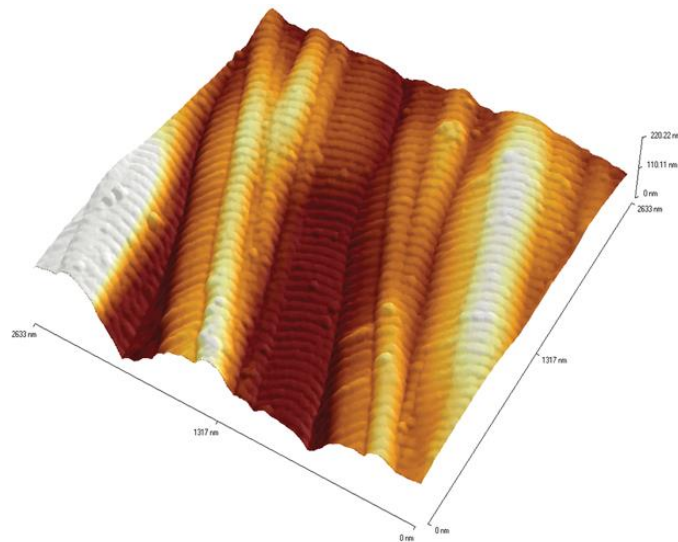


Figure 39- High-Resolution Imaging using Contact Mode

**TappingMode:** Which is the most popular imaging mode, enabled researchers to perform imaging on samples that are too fragile for the Contact Mode. This is a **Bruker**-patented technique that can be used to map the topographies of samples by lightly tapping their surfaces with an oscillating probe tip. The amplitude of these oscillations change based on the topography of the surface and these changes lead to deviations in the position of the cantilever which will be used to image these topographies. [43]

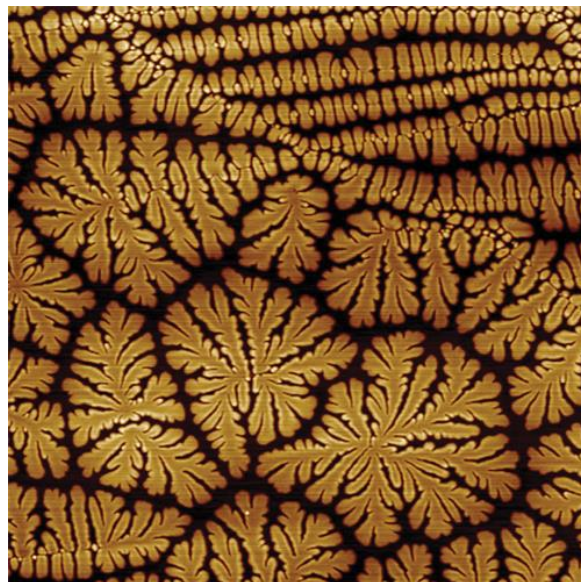


Figure 40- Delicate and Accurate Imaging using the Tapping Mode

**PeakForce Tapping:** Exclusive by **Bruker**, PeakForce Tapping is the most significant breakthrough in AFM technology since the TappingMode. It provides high-resolution in unprecedented levels and enables simultaneous nanoscale property mapping.[44]

These modes can be even divided into more specific sub-modes depending on their use and motives.

As for Nanomechanical modes, they include:

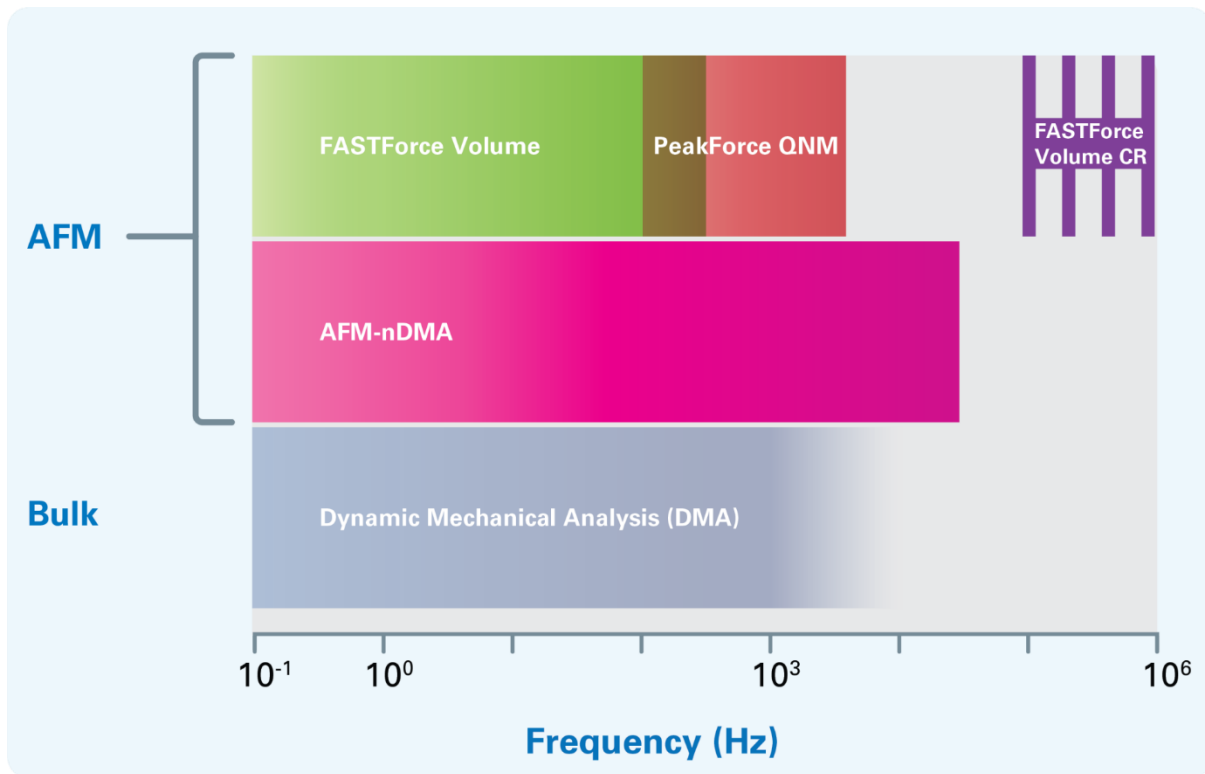


Figure 41- Frequency Used for Different Nanomechanical Modes

**PeakForce QNM:** Which is the mode which we used in our analysis and stands for Quantitative Nanoscale Mechanical characterization. It is used to distinguish between nanomechanical properties like modulus, adhesion, dissipation, and deformation—with up to atomic resolution in topography as well as in the property channels. It can be considered non-destructive to both tip and sample since the peak normal force is controlled thus minimizing the lateral force on the probe.[45]

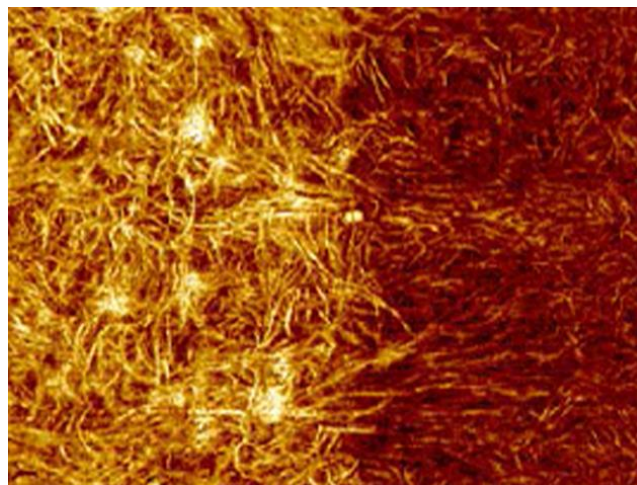


Figure 42- Nanoscale Resolution Imaging using QNM (image size 3  $\mu\text{m}$ )

**AFM-nDMA:** The first and only AFM-based viscoelastic technique that ties directly to bulk Dynamic Mechanical Analysis (DMA). It helps eliminate issues like nonlinearities in the measurements, use of irrelevant frequencies, and subsequent need to ‘recalibrate’ the results, which appear while studying sample stiffness and viscous drag.[46]

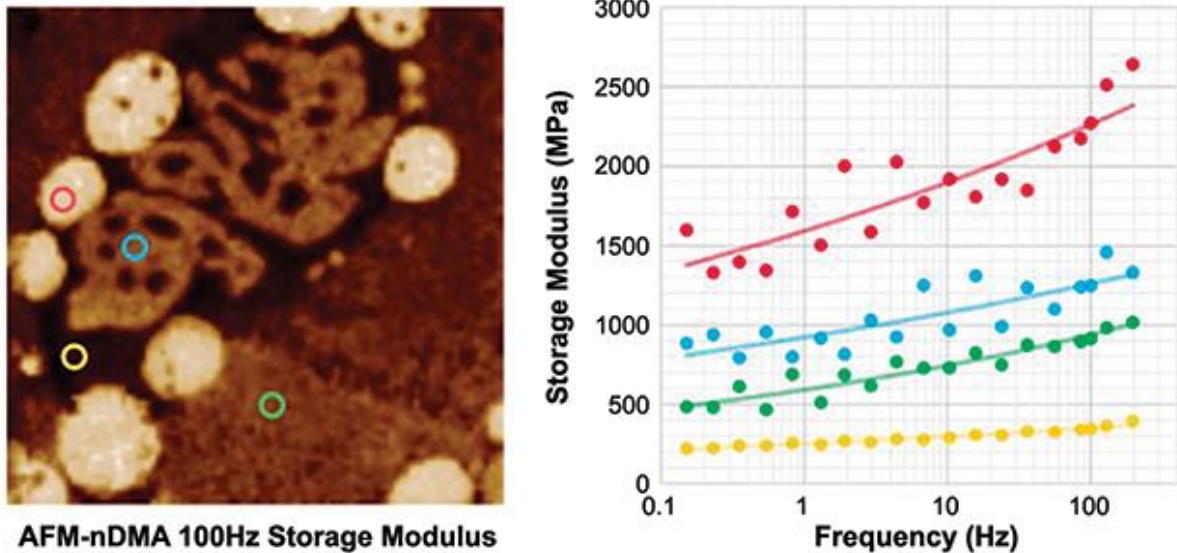


Figure 43- AFM-nDMA Imaging

**FastForce Volume:** Traditional force mapping, more powerful and accessible than ever. It extends the traditional technique reaching ramp rates exceeding 100Hz while maintaining trigger forces in the order of pN. When paired with the PeakForce QNM kit, it can provide quantitative nanomechanical data, without the need of a reference sample.[47]

Other Nanomechanical modes include:

*Force-Distance Measurements*

*Ringing Mode*

*Nanoindenting and Nanoscratching*

*Force Modulation Microscopy (FMM)*

*PhaseImaging Mode*

*Lateral Force Microscopy (LFM)*

There are also Nanoelectrical modes like:

Table 7- NanoElectrical Lab – Techniques and Applications

Techniques	Conductivity	Impedance	Carrier Density	Piezoelectricity	Local EC Activity	Potential/Field
DataCube Mode	DCUBE-TUNA DCUBE-CAFM DCUBE-SSRM	DCUBE-sMIM	DCUBE-SCM DCUBE-sMIM DCUBE-SSRM	DCUBE-PFM DCUBE-CR-PFM	DCUBE-SECM	DCUBE-EFM
PeakForce Tapping (PF)	PF-TUNA	PF-sMIM	PF-sMIM		PF-SECM	PF-KPFM
Tapping Mode		sMIM				EFM KPFM
Contact Mode	TUNA C-AFM SSRM	sMIM	SCM sMIM SSRM	PFM	SECM	
<b>Applications</b>						
Semiconductors	•	•	•			•
Ferroelectrics	•	•	•	•		•
2D materials	•	•				•
Smart materials	•	•		•		•
Piezoelectrics	•	•		•		•
Nanowires and nanoparticles	•	•				•
Photovoltaic	•	•	•			•
Conductive polymers	•	•				•
Battery and fuel cells	•	•		•	•	•
Corrosion studies	•	•			•	•
Dielectrics	•	•				

**Tunneling AFM (TUNA):** Used for Ultra-low current measurement ( $> 1$  pA) on low-conductivity samples with very high current sensitivity , Tunneling AFM (TUNA) can also be used to localize electrical defects in semiconductor or data storage devices, or to study conductive polymers, organics, or other materials. It is especially important to characterize low-conductivity samples at high lateral resolution.[48]



Figure 44- Topography (Left) and Tunneling (Right) Images of an 8.5 nm-Thick SiO<sub>2</sub> Sample. 2 $\mu$ m Scan Size, 200fA Current Scale

**DataCube Modes:** Which gives us multidimensional nanoscale information at every pixel. DataCube modes outspread capabilities (and modes), that can now provide simultaneous capture of nanometer-scale electrical and mechanical characteristics in high-density data cubes for multiple different kind of modes like ‘TUNA’ for example, which was previously impossible to produce in a single measurement.[49]

The list for other nanoelectrical modes can also include:

*Scanning Tunneling Microscopy (STM)*

*Conductive AFM (C-AFM)*

*PeakForce sMIM*

*Kelvin Force Probe Microscopy (KFPM)*

*Scanning Spreading Resistance Microscopy (SSRM & SSRM-HR)*

*Electric Force Microscopy (EFM)*

*Piezoresponse Force Microscopy (PFM)*

*Scanning Capacitance Microscopy (SCM)*

*PeakForce TUNA*

*PeakForce KPFM*

The AFM can also be used for Nanoelectrochemical modes:

*PeakForce SECM*

*Electrochemical AFM (EC-AFM)*

*Scanning Electrochemical Potential Microscopy (SECPM)*

In our case, we utilized the PeakForce QNM mode based off the PeakForce Tapping in order to be able to study some topographic characteristics in addition to our main objective which is to find the adhesion force of the surface of these samples and how it can change in saturated conditions.

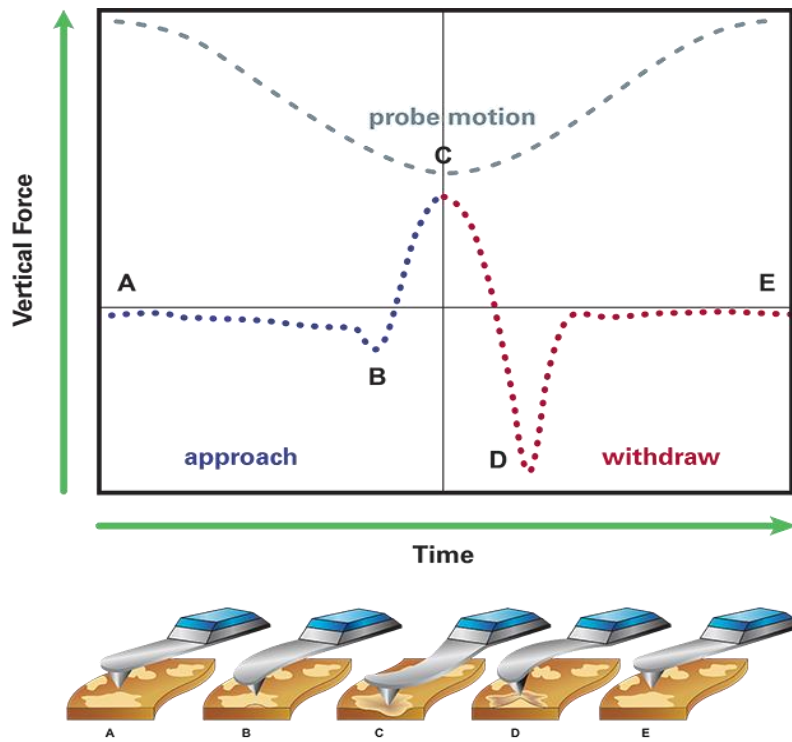


Figure 45- PeakForce Tapping Pattern

We can clearly see three different force application instances at points 'B', 'C', and 'D'.

At point C, we have the applied force exerted on the surface by the tip, to a value which is previously set to be constantly applied by the AFM; however, for points 'B' where we have the approach of the tip towards the surface, and 'D' where the tip is continuing its oscillation trying to detach from the surface after contact was established at point 'C', we have adhesion forces between the surface and the tip.

The adhesion forces, and thus their work, depend directly on the intrinsic surface energy of materials we are working with. This can be directly seen in the Young-Dupre equation:[50];[51]

$$W_A = \gamma_1 + \gamma_2 - \gamma_{12} \quad (23)$$

Where:

$W_A$  = Work of Adhesion

$\gamma_1$  = Surface Free Energy (or surface tension for liquids) of the Material 1

$\gamma_2$  = Surface Free Energy of the Material 2

$\gamma_{12}$  = Interfacial Tension Between Materials 1 and 2

The work of adhesion can be related to the adhesion forces using both the Johnson-Kendall-Roberts (JKR) theory or Derjaguin-Muller-Toporov (DMT) theory by the following equation:[52]

$$\gamma = \frac{F_{adh}}{2\pi cR} \quad (24)$$

Where :

$\gamma$  = Surface Energy

$F_{adh}$  = Measured Adhesion Force

$R$  = Radius of the Tip Used in the AFM

$c = 1.5$  and  $2$  respectively for JKR and DMT models.

These two models describe the geometry of the contact area for which the adhesion force is being calculated.[53]

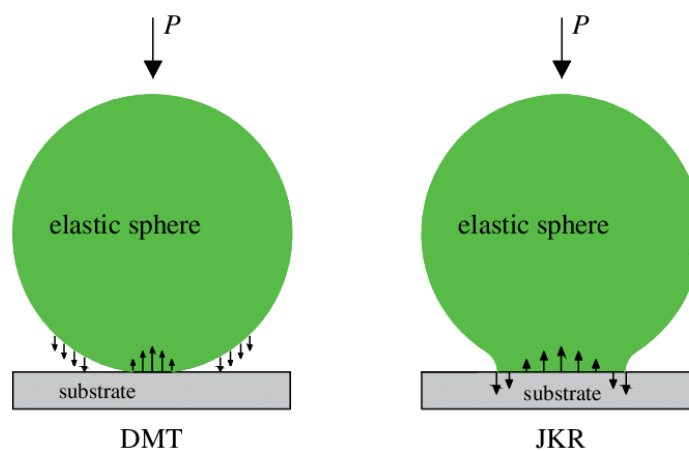


Figure 46- JKR VS DMT[54]

This shows a direct relationship between the adhesion forces and SFE of the materials we are working with; therefore, we decided that by placing a fluid at the point of measurement, and then by changing that fluid, and measuring the change in the adhesion force, we can find the effect that each fluid has on the SFE of the chalk samples.

This is performed by mounting a special probe on the AFM with which In Fluid imaging is possible.

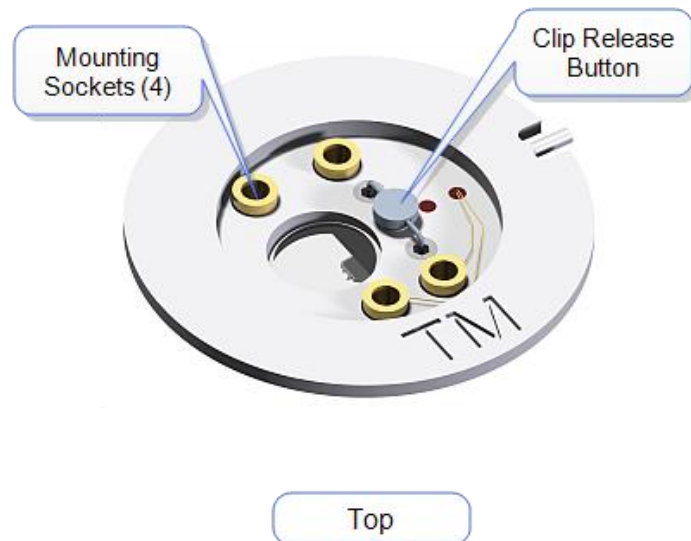


Figure 47- In Fluid Imaging Probe[55]

This would permit to maintain a small ‘liquid cell’ in which the tip and the part of the surface on which we will perform the measurements to remain filled with the fluid of our choice.

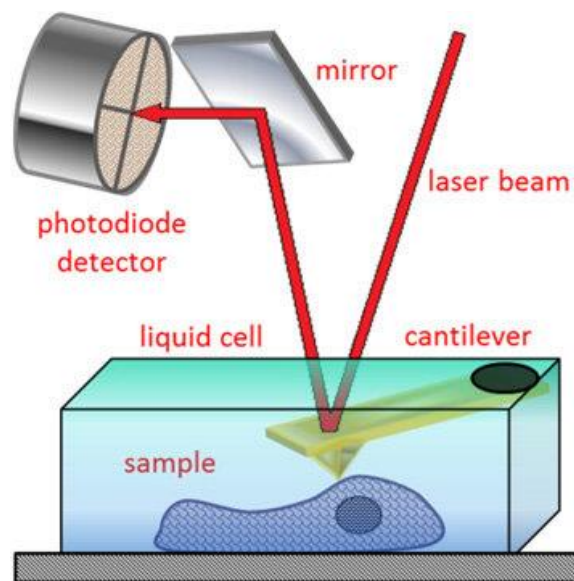


Figure 48- Sketch Representing in Fluid AFM Measurement[56]

However, for the measurements in the dry conditions (in air measurements), there is also the capillary forces. Having the measurements done at a nanoscale and using tips of extremely small dimensions means that it is imperative that capillarity effects will be encountered between the surface of our samples, and the tip of the AFM as it is approaching, resulting in penetration of the tip into the layer of water adsorbed on the surface.[58]

The capillary forces can be estimated by the following equation:[57]

$$F_{cap} = 4\pi R\gamma_{cap} \cos \theta \quad (25)$$

Where:

$F_{cap}$  = Capillary Forces

R = Tip Radius

$\gamma_{cap}$  = Water Surface Energy

$\theta$  = Average Contact Angle values obtained with Deionized Water

Therefore, the adhesion force of the surface of our samples, removing the forces due to the capillarity effects can be calculated by the following equation:

$$\gamma = \frac{F_{adh} - F_{cap}}{4\pi R} \quad (26)$$

The AFM can also be extremely useful when used to measure the roughness of a surface at a nanoscale.

Nonetheless, in our case, knowing that these capillary forces are due to the humidity, of which we do not have any control, we decided to use *eq. (24)* instead of *eq. (26)* to perform the Surface Free Energy Calculations.

Also, in our case we used the saturated samples instead of regular samples due to the fact that the topography in the presence of the pores might be dangerous for the tip as it might erode it which will cause a significant loss.

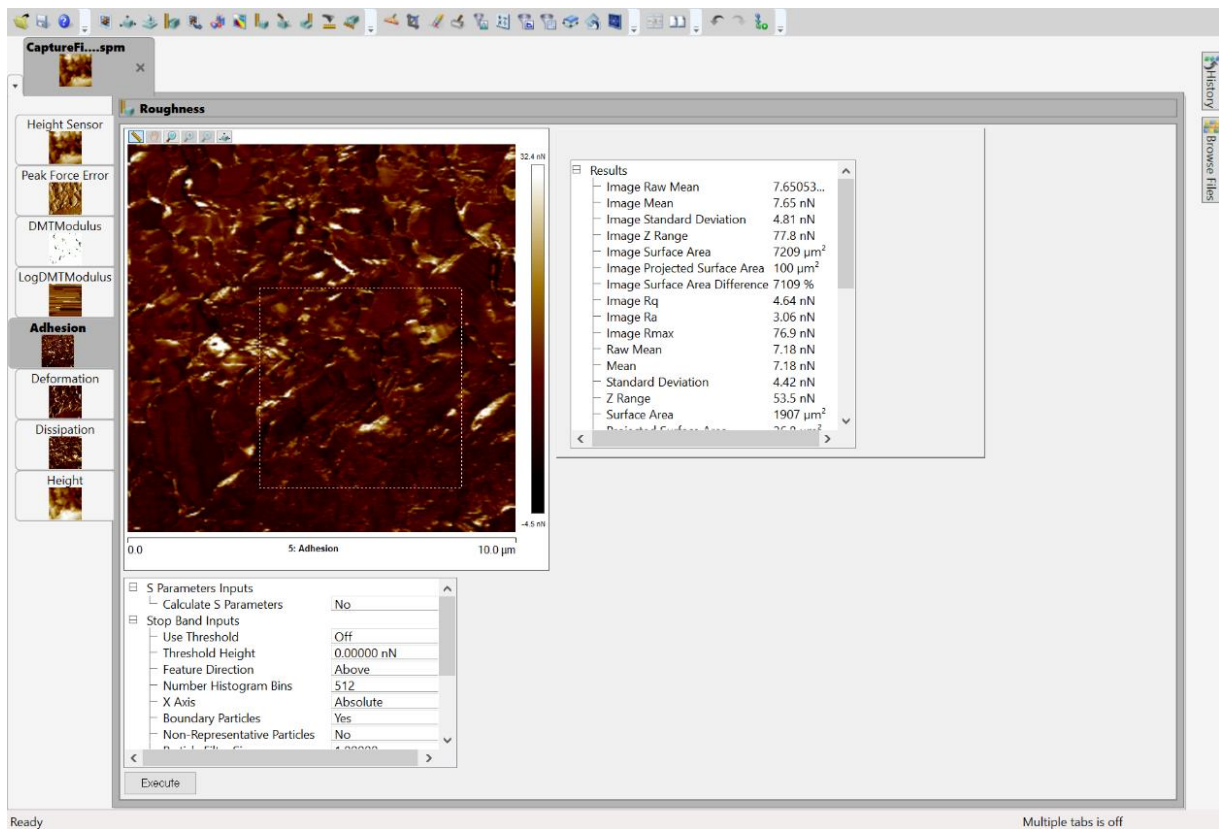


Figure 49- DATA Acquired Using the PeakForce QNM Visualized Using the NanoScope Analysis 2.0 Software

However, in our case we preferred to use the Confocal Laser Scanning Microscopy, since as clearly visible in *Figure 49*, the AFM produces measurements over a very small area ( $10 \mu\text{m} \times 10 \mu\text{m}$ ) with a considerable amount of time required for each scan, whereas in the case of the confocal it is feasible for approximately the same amount of time, and even less, to acquire an image along the lines of *Figure 20*, which showcases an area that is at least four hundred times bigger than that which is produced by the AFM.

Moreover, in *Figure 49* we can see that using the NanoScope Analysis 2.0 software to visualize the data acquired by the AFM, we can have a big collection of data which we can manipulate and use to better understand our samples. We can view an image showing the distribution of the adhesion force throughout the measured part of our samples or use the height sensor tab to get an idea about the topography we are working with in our sample. Furthermore, we can get all these data not only for the measured part, but we can also get average values for specific windows chosen by us from the entire image, this way if we have some doubts about how the topography might for example affect the adhesion force measurement on one side or the other, we can simply chose another window without that part, or just choose a specific part in which we are sure that the data we are obtaining truly reflects the areas at which we are sure to get the values we desire.

# 3.Results

## 3.1. O.W.R.K Model on Chalk

Initial testing was performed on Preliminary Samples during the sample preparation stage in order to make sure that the procedure we were following was up to standards to give us the results that we wanted.

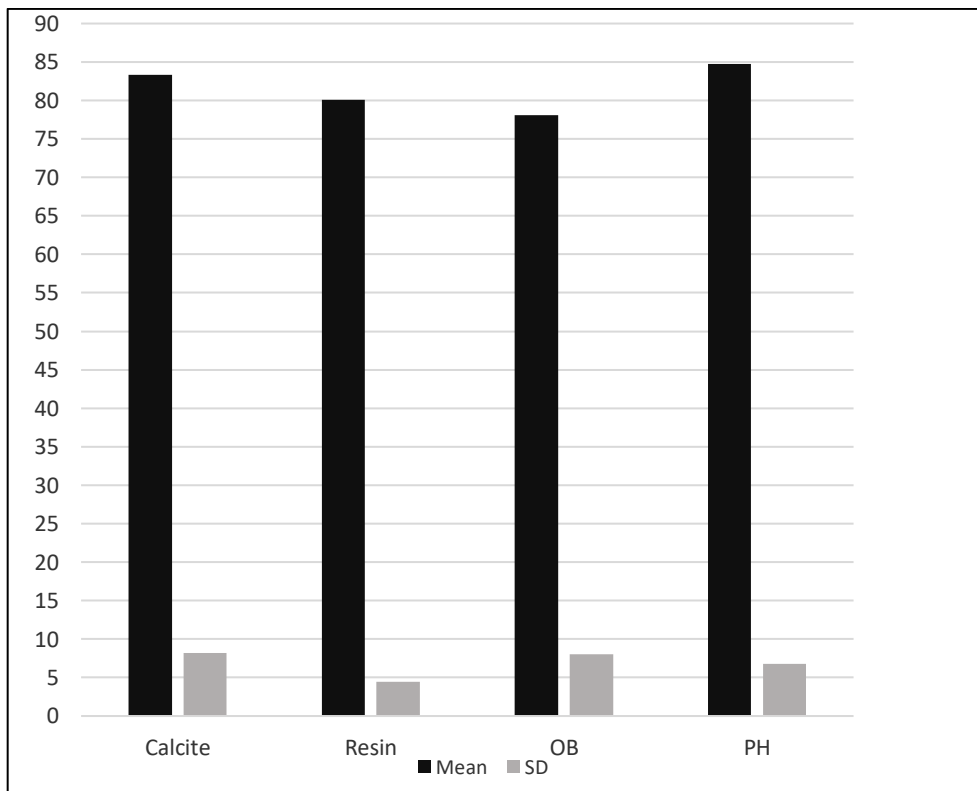


*Chart 1- Contact Angle Values of Ultra-Pure Water*

*Chart 1* compares the average contact angle values of Ultra-Pure water on different kinds of samples.

*Table 8- Mean Contact Angle Values of Ultra-Pure Water*

-	Calcite	Resin	OB	PH
Mean	83.36	80.1	78.12	84.74
SD	8.19	4.42	8.06	6.75

These values are provided from doing contact angle measurements on Pure Resin samples, Obourg (OB) Chalk samples, Phosphatic Ciply (PH) Chalk samples, and Pure Calcite Samples.

We can clearly see in *Chart 1* and *Table 8* that these values are very much close to each other, and this actually was one of the main reasons that pushed us towards enhancing our preparation as these close values lead to us doubting that our preparation was faulty and perhaps there was a small layer of Resin from the Saturation Process still existing on the surface of our samples and influencing the contact angle measurements of our samples.

Upon enhancing our preparation procedure, we needed to decide on the most suitable Sample Liquids with which we can perform the O.W.R.K Model.

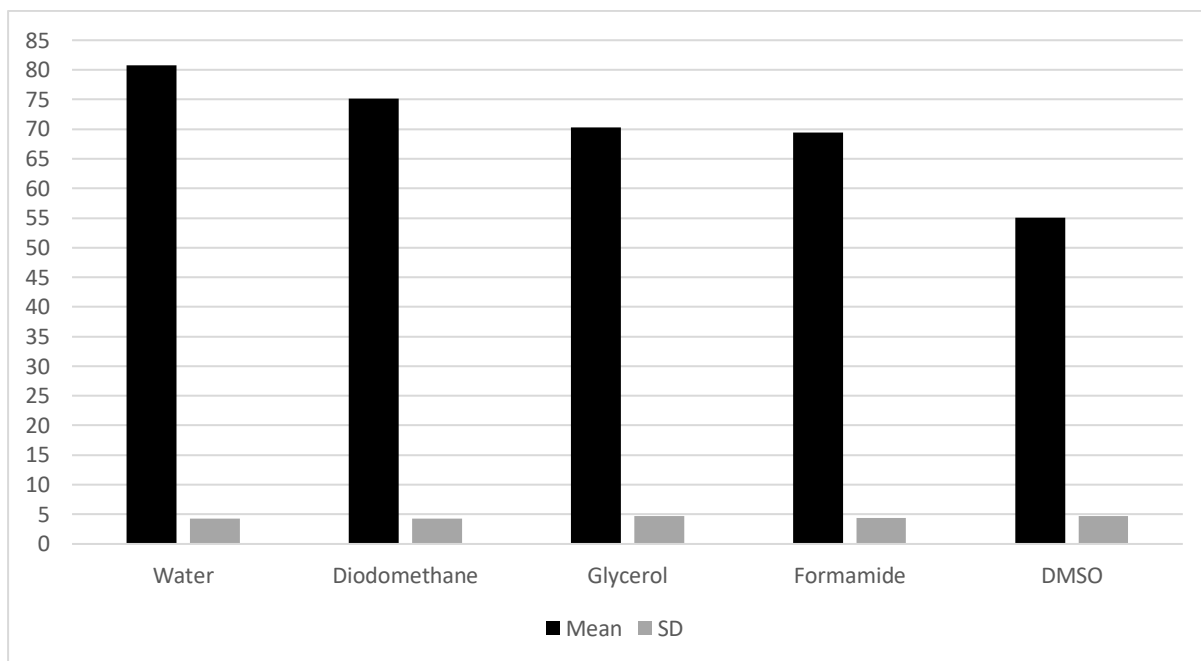


*Chart 2- Contact Angle Values of Sample Liquids on Pure Resin*

We decided that another way to test the reliability of the Sample Liquids we chose was to ensure that they can show a certain pattern of values on the pure resin contact angle measurements which might help eliminate the main factor that drove us towards enhancing the preparation of our samples in the first place: Acquiring Close Values.

*Table 9- Mean Contact Angle Values on Pure Resin Samples*

-	Water	Diodomethane	Glycerol	Formamide	DMSO
Mean	80.73	75.16	70.32	69.46	55.06
SD	4.23	4.23	4.76	4.4	4.75

After ensuring that we have reached an ideal level of preparation for the samples and have properly chosen our sample liquids with which we can perform the contact angle measurements properly, we can finally proceed with the O.W.R.K Model.

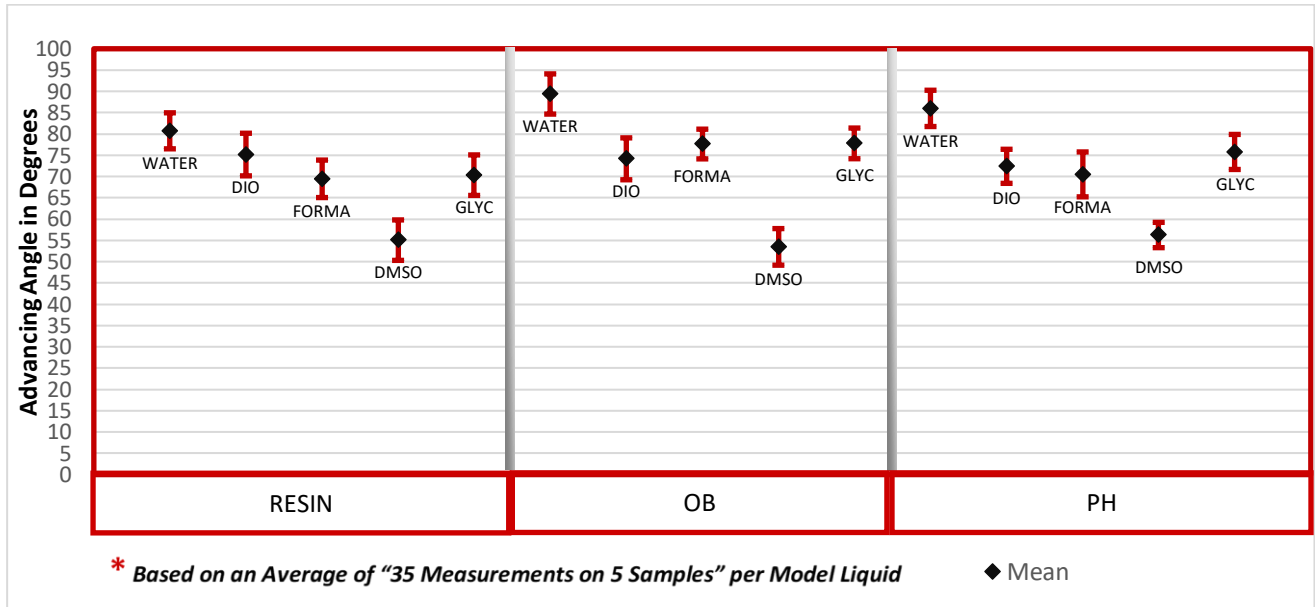


Chart 3- Obtained Means\* of the Advancing Angle Measurements

These are the values obtained after performing a total of 467 advancing contact angle measurements using all Five Sample Liquids: Ultra-Pure Water (WATER), Diiodomethane (DIO), Formamide (FORMA), Dimethyl Sulfoxide (DMSO), and Glycerol (GLYC); these measurements were done on samples made of Pure Resin (RESIN), Saturated Obourg Chalk (OB), Saturated Ciply Phosphatic Chalk (PH).

Table 10- Average and Standard Deviation Values of all Contact Angle Measurements Including Porosity( $\phi$ ) Values

$\phi$	-					0.4344	0.4344	0.4344	0.4344	0.4344	0.3887	0.3887	0.3887	0.3887	0.3887
Measurements	Resin					OB					PH				
Fluid	Water	Diodomethane	Formamide	DMSO	Glycerol	Water	Diodomethane	Formamide	DSMO	Glycerol	Water	Diodomethane	Formamide	DMSO	Glycerol
Mean	80.73404255	75.16	69.46	55.06	70.31714	89.38	74.16	77.632	53.476	77.784	86	72.4	70.5	56.26667	75.77333
SD	4.23	5	4.4	4.75	4.758243	4.72	4.92	3.49	4.3	3.603202279	4.26	4	5.27	2.970468	4.11565

As can be clearly seen from *Chart 3* and *Table 10*, we only have relatively small values in terms of the standard deviation viewed by values ranging between three and five degrees, which is acceptable mainly considering we are working with rock samples whose heterogeneities make it near impossible to have completely homogeneous samples.

After that, we wanted to make sure that the roughness of the surfaces of our samples are not affecting the measurement using the Confocal Laser Scanning Microscope under both x20 and x40 Zoom settings.

Table 11- Roughness Measurement of Chalks

Chalk	OB	PH
Zoom 40x	0.92	0.85
Zoom 20x	0.86	1.71
Mean (µm)	0.89	1.28
SD	0.06	0.61

As we can clearly see in *Table 11*, the values of the roughness Ra. of the Obourg Chalk are less than 1 µm which is ideal, whereas the slight increase in the values for the Cibly Phosphatic Chalk is due to some troughs on the surface which are the result of minerals of a larger size (with respect to the matrix) which might have been detached during the preparation process. Nonetheless, both values suggest a successful polishing procedure.

The first step now is separating the effects of the resin by using the Cassie-Baxter equation (*eq. (3)*) to eventually obtain contact angle values of each of our Sample Liquids on our Cibly and Obourg chalk samples.

Table 12- The Cosine of the Contact Angle on the Pure Chalk

Cassie's Law	OB					PH				
cos(θ)	-0.18473904	0.294866683	0.036240131	0.624378403	0.048564	-0.07376767	0.375105037	0.306985844	0.52797953	0.102558356
FLUID	WATER	DIO	FORMA	DMSO	GLYC	WATER	DIO	FORMA	DMSO	GLYC

We decided to directly calculate the Cosine of the contact angle instead of the angle itself since it is the value required later on in the O.W.R.K Model calculations.

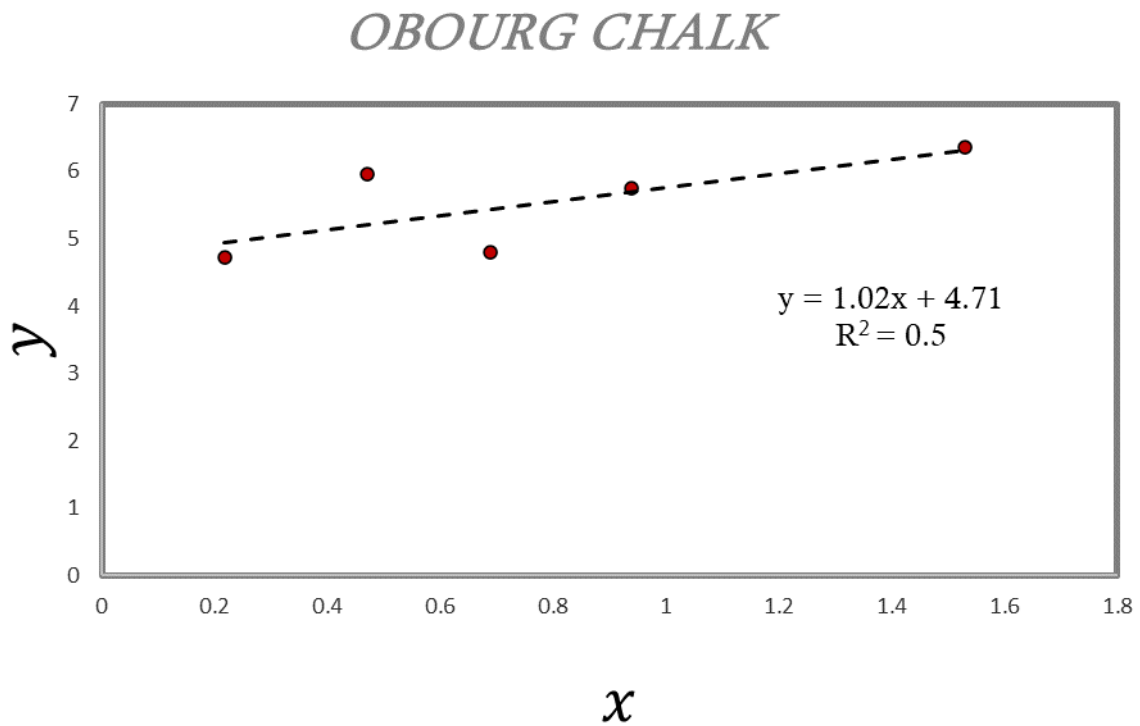
The next step is to try to reformulate *eq. (10)* and to calculate the values for the abscissa axis by

$$x = \frac{\sqrt{\gamma_{lv}^p}}{\sqrt{\gamma_{lv}^d}} \text{ and for the ordinate axis by } y = \frac{\gamma_{lv} \cos\theta_Y - 1}{2\sqrt{\gamma_{lv}^d}} .$$

Table 13- Final O.W.R.K Model Calculations for Obourg Chalk

OB	WATER	DIO	FORMA	DMSO	GLYC
DISP $\gamma^d$	21.8	48.5	39.5	36	34
POL $\gamma^p$	51	2.3	18.7	8	30
TOT $\gamma$	72.8	50.8	58.2	44	64
$1+\cos(\Theta)$	0.81	1.29	1.04	1.62	1.05
$x$	1.53	0.22	0.69	0.47	0.94
$y$	6.36	4.72	4.8	5.96	5.75

Each Sample Liquid, and the contact angle measurements with these liquids, will allow us to have one point. The Owens–Wendt method usually requires the advancing contact angle measurements with a minimum of two liquids, an apolar one and a polar one. However, the larger the set of Sample Liquids used, the better accuracy in the SFE determination.[59]



Graph 4- O.W.R.K Model for Obourg Chalk

The Best-Fit Linear line resulting from these points is then used to calculate the SFE.

The intercept of this line, which corresponds to  $\sqrt{\gamma_{sv}^d}$ , is calculated to be 4.71, while the slope which represents  $\sqrt{\gamma_{sv}^p}$  is determined as 1.02. The values are then found of the polar and dispersive components of the Surface Free Energy and put into eq. (7).

Table 14- SFE of Obourg Chalk

$\gamma^d$	22.2
$\gamma^p$	1.04
<b><math>\gamma</math> (mN/m)</b>	23.2

The OW.R.K Model provides us with an Surface Free Energy Value for Obourg Chalk which is equal to 23.2 mN/m (0.0232 J/m<sup>2</sup>).

This Model was also applied for the Ciplly Phosphatic Chalk in order to be able to get the Surface Free Energy.

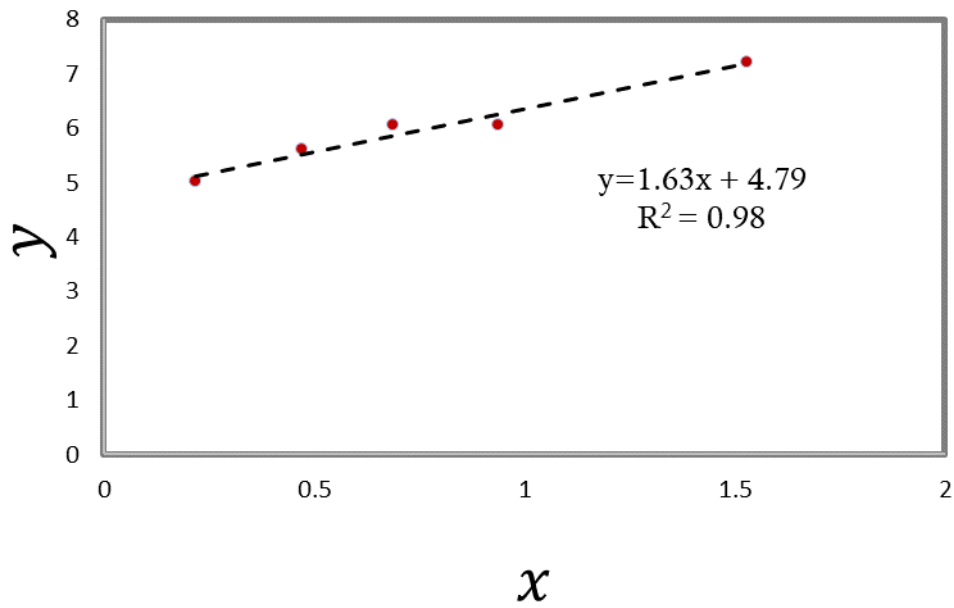
Table 15- Final O.W.R.K Model Calculations for Ciplly Phosphatic Chalk

PH	WATER	DIO	FORMA	DMSO	GLYC
DISP $\gamma^d$	21.8	48.5	39.5	36	34
POL $\gamma^p$	51	2.3	18.7	8	30
TOT $\gamma$	72.8	50.8	58.2	44	64
$1+\cos(\Theta)$	0.93	1.37	1.31	1.53	1.1
$x$	1.53	0.22	0.69	0.47	0.94
$y$	7.22	5.01	6.05	5.6	6.05

These calculated data were then input to use the O.W.R.K Model.

The results with the Ciplly Phosphatic Chalk produce some very nice results including a very good fitting as shown by an R-squared value equals to 0.98 in Graph 6 below:

## *PHOSPHATIC CHALK*



*Graph 5- O.W.R.K Model for Ciply Phosphatic Chalk*

Again, by finding the slope and the intercept, we can extrapolate both the dispersive and polar components, and calculate the SFE.

*Table 16- SFE of Ciply Phosphatic Chalk*

$\gamma^d$	22.95
$\gamma^p$	2.65
<b><math>\gamma</math> (mN/m)</b>	25.6

As for the Ciply Phosphatic Chalk, the O.W.R.K Model shows that the value of its Surface Free Energy is equal to 25.6 mN/m (0.0256 J/m<sup>2</sup>).

### 3.2. O.W.R.K Model on Calcite

In an attempt to try and verify the Surface Free Energy values we obtained in the O.W.R.K Model, we decided that the next step should be to use the same model, but this time on pure calcite minerals already available at the Laboratory.

*Table 17- Average and Standard Deviation Values of Contact Angle Measurements on Calcite*

Fluid	Water	Formamide	Diiodomethane
Mean	77.76	73.75	71.25
SD	4.89	7.09	3.46

The difference is that for the pure calcite minerals, we can avoid the saturation process, and thus we do not need to use the Cassie-Baxter equation, as the sample we are performing the test on is homogenous (no resin since we do not have pores that we needed to fill).

Roughness Ra. measurements were also performed on the surfaces of the calcite samples using the Confocal Laser Scanning Microscope using the x20 Zoom setting:

*Table 18- Roughness Measurements of Calcites*

Calcite	Big	Small
Ra. ( $\mu\text{m}$ )	3.42	2.12

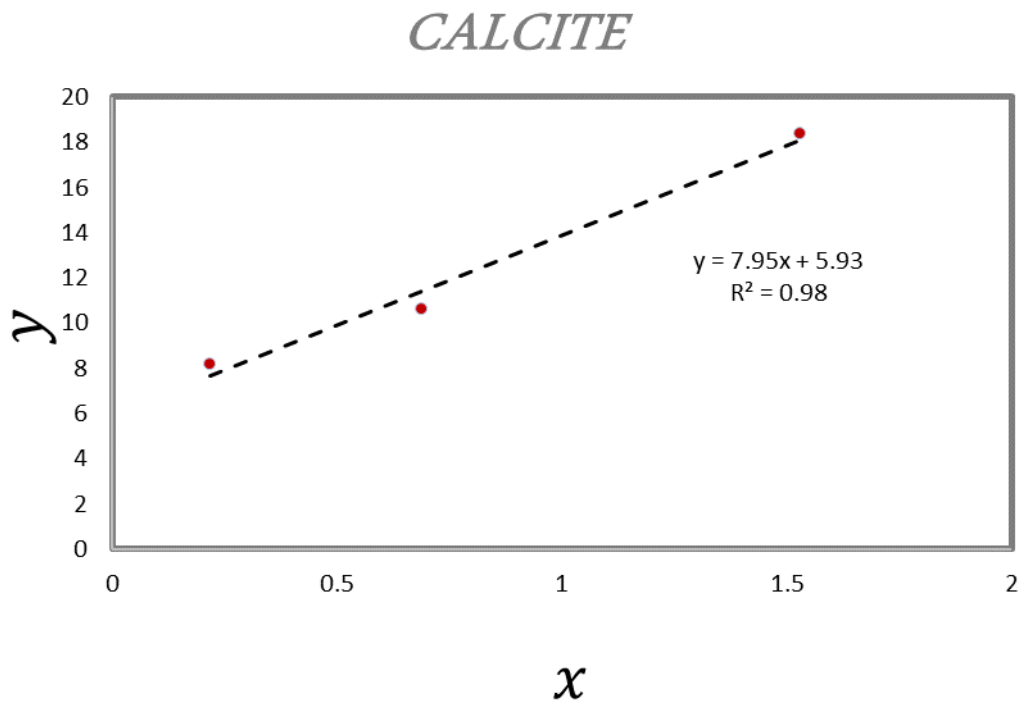
The values are slightly higher than those of the prepared chalk samples, however they are still acceptable values.

*Table 19- Final O.W.R.K Model Calculations for Calcite*

CALC	WATER	DIO	FORMA
DISP $\gamma^d$	21.8	48.5	39.5
POL $\gamma^p$	51	2.3	18.7
TOT $\gamma$	72.8	50.8	58.2
$1+\cos(\Theta)$	2.36	2.24	2.29
$x$	1.53	0.22	0.69
$y$	18.38	8.18	10.59

The average values obtained from the Contact Angle Measurements were directly input into eq. (10) to use the O.W.R.K Model.

In the case of the calcite mineral, we only performed measurements with a range of only three Sample Liquids due to the limited amount of time available. These Sample Liquids were Diiodomethane, Formamide, and Ultra-Pure Water.



*Graph 6- O.W.R.K Model for Calcite*

The O.W.R.K Model with the calcite has provided us with a great fitting of points on the trendline, with a very good R-squared Value of only 0.98 just like in the case of the model with the Ciply Phosphatic Chalk.

*Table 16- SFE of Calcite*

$\gamma^d$	35.2
$\gamma^p$	63.14
<b><math>\gamma</math> (mN/m)</b>	98.34

We can see that the O.W.R.K Model on Calcite Minerals has provided us with a Surface Free Energy value of 98.34 mN/m which is different than the those of the chawks, yet still in the same order of Magnitude.

### 3.3. SCB

Comparing these values to the Surface Fracture Energy values regularly found in the literature for Calcite minerals, we noticed a big difference. We should also note that these values usually found are calculated based on a different methodology which usually involves crack propagation mechanisms.

This led us to try and calculate the Surface Free Energy of our two Chalks in a mechanical method that also depends on crack propagation mechanisms to try and decipher the discrepancy between the values that we obtained, and the values found in the literature. So, we performed the SCB Test and calculate the fracture energy using the Mode I Fracture Toughness ( $K_{Ic}$ ) of our chalk samples. These tests were carried out over a total of twenty Obourg Chalk samples, and six Ciply Phosphatic Chalk samples, divided into groups, each tested under different conditions.

For the Obourg, we had four samples tested in dry conditions, including one which was used a test run, but whose value was later found to be acceptable, while for the Ciply Phosphatic Chalks there were three. These samples remained in the oven for more than forty-eight hours at a temperature of fifty degrees Celsius.

The other samples were all tested under saturated conditions. They were put through the saturation set-up shown in *Figure 36*. Four Obourg Chalk samples, as well as the remaining three Ciply Phosphatic Chalk samples were saturated with deionized water, while the rest of the Obourg samples were divided into groups of three, and each group was saturated with one of the following solutions before testing: NaCl - CaCl<sub>2</sub> - MgCl<sub>2</sub>. All these saturating solutions were prepared having different mass concentrations, but at the same time having an equivalent Ionic Strength at a value of 0.598.

After Saturation, but before the SCB testing, the mass of the samples was measured in order to calculate the porosity using *eq. (20)* so that we can check for any anomalies that would appear in the form of inaccurate porosity values.

Table 20- Porosity Measurements for Obourg SCB Samples

Sample	Solution	$m_{Dry}$	$m_{Imm}$	$m_{Sat}$	$\phi$
OS4	DeIonized Water	33.86	21.32	42.99	0.421
OS5		34.53	20.49	41.51	0.332
OS6		36.06	22.72	45.66	0.419
OS19		32.06	20.2	40.78	0.423
OS7	NaCl 35 g/L	39.31	24.36	50.02	0.417
OS8		31.32	19.39	40.04	0.422
OS9		33.23	20	42.57	0.414
OS10	MgCl <sub>2</sub> 19 g/L	32.2	20.1	40.8	0.415
OS11		30.9	19.29	39.5	0.425
OS12		29.47	18.39	37.84	0.43
OS13	CaCl <sub>2</sub> 22.15 g/L	31.5	19.63	40.15	0.422
OS14		28.55	17.8	36.39	0.422
OS15		32.34	20.16	41.38	0.426
Ionic Strength	0.598	g			0.421
					Average $\phi$

Our only anomaly appearing in the form of the Obourg Sample OS5 which was saturated with deionized water, all the other samples displayed acceptable values,

After the preparation and the check-up were accomplished, we performed the SCB Tests.

But in order to calculate the Fracture Energy, we also needed other factors, such as the Poisson's Ratio, and the Young's Modulus. For the Obourg Chalk, we used values obtained from another internship student at the same laboratory who performed the required tests, whereas for the Cibly Phosphatic Chalk we need to perform some UCTs.

Table 21- UCTs

Sample	Condition	E (GPa)	$E_{avg}$ (GPa)
P7	Dry	1.63	1.185
P8		1.33	
P9		0.913	
P10		1.034	
P12		1.122	
P15		1.974	
P21		0.641	
P13		0.746	
P19		0.546	
P18		1.919	
P22		DeIonized Water	
P23	0.837		
P24	0.413		
P25	0.402		

The results show a significant difference in the values of the Young's Modulus of the dry and saturated samples.

These values are then input to use in the calculation of the Fracture Energy, according to *eq. (19)* since we did not measure Poisson's ratio in our rocks.

Table 22-  $K_{Ic}$  and  $\gamma$  Values for Ciplly Phosphatic Chalk

Name	Saturation	E (GPa)	$K_{Ic_{avg}}$ (MPa)	$\gamma_{F_{avg}}$ (mN/m)
PS1 L	DRY	1.185	0.053	<b>1023.8</b>
PS2 M				
PS3 S				
PS4 L	DeIonized Water	0.495	0.027	<b>846.5</b>
PS5 M				
PS6 S				

Table 23-  $K_{Ic}$  and  $\gamma$  Values for Obourg Chalk

Name	Saturation	E	$K_{Ic_{avg}}$	$\gamma_{F_{avg}}$
TEST	DRY	5480	0.084	<b>609.9</b>
OS1	DRY	5480	0.071	<b>434.15</b>
OS2				
OS3				
OS4	DeIonized Water	3170	0.05	<b>378</b>
OS5				
OS6				
OS19				
OS7	NaCl	2760	0.037	<b>244.3</b>
OS8				
OS9				
OS10	MgCl <sub>2</sub>	3780	0.05	<b>240.9</b>
OS11				
OS12				
OS13	CaCl <sub>2</sub>	3750	0.046	<b>268.18</b>
OS14				
OS15				
Ionic Strength	0.598	MPa		<b>mN/m</b>

These values are comparable and of the same order of magnitude as the values found in the literature:

Table 24- Literature Surface Energy Results of Calcites[28]

Reference	$\gamma_{s, Dry}^e$ (J/m <sup>2</sup> )	$\gamma_{s, Wet}^e$ (J/m <sup>2</sup> )
<i>Experimental Results<sup>a</sup></i>		
This study	0.32	0.15
Donnet et al. [2005]		0.046 ± 0.007
Donnet et al. [2005]		0.135 ± 0.029
Donnet et al. [2009]		0.039–0.164
Gilman [1960]	0.23	
Santhanam and Gupta [1968]	0.347 ± 0.045	

Where the values are in (J/m<sup>2</sup>) which corresponds to 1000 (mN/m).

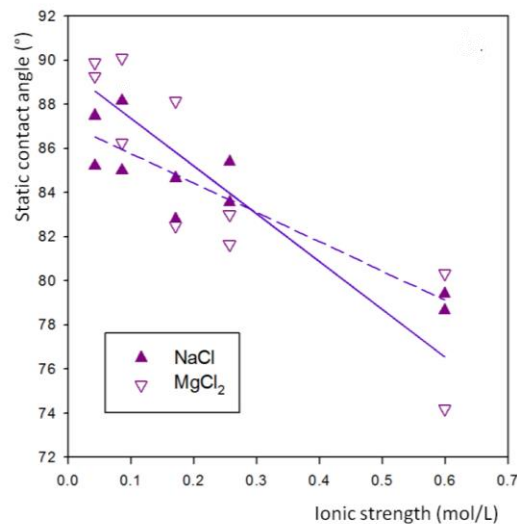
### 3.4. Brine Contact Angle Measurements on Calcites

Now to measure the change of wettability as an effect of different solutions (and of different concentrations) interacting on the surface of our calcite samples, we performed the contact angle measurements in Static mode which gave us the results in *Table 25* below:

*Table 25- Average Values of Contact Angle Measurements for Each Brine*

Brines	Salinity (mol/L)	Sample 1	Sample 2
NaCl	0.075	87.48	85.2
	0.15	88.16	85
	0.3	84.66	82.8
	0.45	83.56	85.4
	1.05	78.66	79.42
MgCl <sub>2</sub>	0.04	89.28	89.88
	0.08	86.26	90.1
	0.16	82.5	88.14
	0.24	81.66	83.02
	0.57	74.2	80.34

These values were then arranged in a way that we can see a pattern that clearly defines the effect of changing the concentration (ionic strength) in terms of the contact angle.



*Graph 7- Contact Angle Measurements vs. Ionic Strength for NaCl and MgCl<sub>2</sub> Brines in Contact with a Single Calcite Crystal [59]*

These results shown in *Graph 4* display a decreasing trend of the Static Contact Angle versus ionic strength which is comparable for both the NaCl and the MgCl<sub>2</sub>.

This shows a clear qualitative effect that a change in concentration can have on the surface properties of the samples in use like the wettability and eventually the Surface Free Energy.

### 3.5. AFM

As for the AFM, we performed the measurements to get the following values.

*Table 26- AFM SFE*

SFE	Air Cell	Liquid Cell
OB	20.74	16.5
PH	19.6	14.07
	mN/m	

We can clearly see a drop in the SFE values as we go from dry to wet conditions, due to the interaction of the water with the surface of our samples.

## 4. Discussion

An extensive dataset has thus been provided in a way that might help us verify the credibility of the surface energy calculations made by the O.W.R.K Model and how the surface energy is affected in the presence of fluids.

Table 27- Surface Energy

		Surface Energy (mN/m)		
Saturation		SCB	AFM	O.W.R.K
PH	Dry	1023.8	19.6	25.6
	WATER	846.5	14.07	-
OB	Dry	478.1	20.74	23.22
	WATER	378	16.5	-
	NaCl	244.3	-	-
	MgCl <sub>2</sub>	240.9	-	-
	CaCl <sub>2</sub>	268.2	-	-
CALCITE	Dry	-	-	98.33

As we can see in *Table 27*, the SFE values of obtained from the AFM and the O.W.R.K Model are slightly different, yet of the same order. This confirms the idea that the surface energy should actually be divided into two completely different types:

Fracture Surface Energy

Surface Free Energy

The true SFE should be dependent on the intrinsic properties of each material which in the case of our experiments is highlighted in the AFM and O.W.R.K Model measurements.

These measurements were mainly dependent on the interaction of these chalk in and out of itself with the tip, in the case of the AFM, and with the Sample Liquids in the case of the O.W.R.K Model. These interactions which are mainly dependent on the characteristic (intrinsic) properties of the samples we are working with since they mainly depend on the molecular interactions within the samples themselves on an atomic level whereby the atoms on the surface would be lacking a bond which would create this potential on the surface due to all those negative and positive charges (depending on the atom which is at the surface at each point and its ion form). This potential would lead to a surface charge and the SFE. Therefore, the existence of a Surface Free Energy lies in the word **FREE**

which describes the main -but not only- factor on which this energy depends: the **FREE** bonds from the atoms on the surface.

On the other hand, we have the Fracture Surface Energy (also described as Fracture Energy) which is defined as the work necessary per unit area to produce a new surface.

The fracture energy is then the energy which is measured by techniques that depend on Crack propagation like the SCB, and which should essentially be treated as a completely different type of energy than the SFE.

We can also notice the impact of having a liquid interaction on the surface energy values. Clearly the decrease in the energy values which applies for all our cases which shows the water-weakening effect.

We can also see from the SCB values that having solutions, instead of just deionized water can cause an even further decrease in the values showcasing that the ionic interaction might also play a role in water-weakening effects. This result is also viewed in terms of the wettability showing that the ions (and their concentrations) do play a role in altering both the Surface Free Energy and the Surface Fracture Energy, which can also be thus linked to an effect on the water-weakening mechanism.

## 5. Conclusion

The O.W.R.K Model, which is rarely used to calculate the Surface Free Energy of rocks (whose porosity usually makes it hard or even impossible to perform the contact angle measurements) has proven successful in this case, validated by the matching results also obtained the Atomic Force Microscopy measurements.

We have also confirmed the validity of differentiating the two Surface Energy annotations since we successfully calculated two different values of surface energy using three different techniques that proved that the values retrieved by the SCB or other crack propagation methodology are actually those of Surface Fracture Energy, and that those retrieved by the AFM, or O.W.R.K Model are values that correspond to the Surface Free Energy.

Another point was made by showcasing that the presence of water, or brines, can actually have an effect decreasing the surface energy values, thus by definition making it easier to create fractures and propagate them in our rocks which shows a weakening of the mechanical properties of the samples verifying the Water-weakening phenomenon is related to the changes in the surface energy.

Further studies are always needed to arrive at a level of understanding of this phenomenon and how we can control it, using the surface energy or other techniques, so that we can use it in favor of enhancing the production by understanding how the reservoir in which it exists reacts.

# References

- 1- Geary, P. & Dillingham, G.. (2021, March). What is the Difference Between Surface Free Energy and Surface Energy? *BTG LABS*. <https://www.btglabs.com/blog/what-is-the-difference-between-surface-free-energy-and-surface-energy>
- 2- Surface Free Energy  
<https://www.nanoscience.com/techniques/tensiometry/surface-free-energy/>
- 3- Surface Energy. (2021, June 8). <https://chem.libretexts.org/@go/page/183363>
- 4- Pahlmann, G. A. (1970). Fracture surface energy determinations of high density polycrystalline ceramics.m
- 5- Zaitsev, Y. B., & Wittmann, F. H. (1981). Simulation of crack propagation and failure of concrete. *Matériaux et Construction*, 14(5), 357-365.
- 6- Wittmann, F. H., Sun, Z., & Zhao, T. (2010, May). Surface energy and fracture energy. In *Proceedings of the 7th International Conference on Fracture Mechanics of Concrete and Concrete Structures, Jeju, Korea* (pp. 13-18).
- 7- Wittmann, F. H., Zhang, P., & Zhao, T. (2006). Influence of combined environmental loads on durability of reinforced concrete structures. *Restoration of Buildings and Monuments*, 12(4), 349-362.
- 8- Godefroit, Pascal. *Bernissart Dinosaurs and Early Cretaceous Terrestrial Ecosystems*. Indiana, Indiana University Press, 2012.
- 9- Moreau, L., Brandl, M., Filzmoser, P., Hauzenberger, C., Geomaere, E., Jadin, I., ... & Schmitz, R. W. (2016). Geochemical Sourcing of Flint Artifacts from Western Belgium and the German Rhineland: Testing Hypotheses on Gravettian Period Mobility and Raw Material Economy. *Geoarcheology*, 31(3), 229-243.
- 10- Robaszynski F, Dhondt AV, Jagt JWM (2002) Cretaceous lithostratigraphic units (Belgium). *Geol Belgica*. <https://doi.org/10.20341/gb.2014.049>
- 11- Voake T, Nermoen A, Ravnås C et al (2019) Influence of temperature cycling and pore fluid on tensile strength of chalk. *J Rock Mech Geotech Eng*. <https://doi.org/10.1016/j.jrmge.2018.12.004>
- 12- Geremia, D., David, C., Descamps, F., Menéndez, B., Barnes, C., Vandycke, S., ... & Sarout, J. (2021). Water-Induced Damage in Microporous Carbonate Rock by Low-Pressure Injection Test. *Rock Mechanics and Rock Engineering*, 1-22.

- 13- Faÿ-Gomord O, Soete J, Katika K et al (2016) New insight into the microtexture of chalks from NMR analysis. *Mar Pet Geol.* <https://doi.org/10.1016/j.marpetgeo.2016.04.019>
- 14- Robaszynski, F.; Martin, M. Late Cretaceous Phosphate Stratiform Deposits of the Mons Basin (Belgium). *Miner. Depos. within Eur. Community* **1988**, 515–529. [https://doi.org/10.1007/978-3-642-51858-4\\_28](https://doi.org/10.1007/978-3-642-51858-4_28).
- 15- Contact Angle: A Guide to Theory and Measurement (2021) <https://www.ossila.com/pages/contact-angle-theory-measurement>
- 16- Laurén, S. (2019, June 11). How to measure contact angle hysteresis and roll-off angle by tilting method? *Biolin Scientific.* <https://www.biolinscientific.com/blog/how-to-measure-contact-angle-hysteresis-and-roll-off-angle-by-tilting-method>
- 17- T.T. Chau; W.J. Bruckard; P.T.L. Koh; A.V. Nguyen (2009). *A review of factors that affect contact angle and implications for flotation practice.* , 150(2), 106–115. doi:10.1016/j.cis.2009.07.003
- 18- Paul, C. (2014, April 22). What is Confocal Laser Scanning Microscopy? BiteSizeBio. <https://bitesizebio.com/19958/what-is-confocal-laser-scanning-microscopy/>
- 19- Laurén, S. (2020, June 09). Wenzel equation – How roughness is related to wettability? *Biolin Scientific.*<https://www.biolinscientific.com/blog/wenzel-equation-how-roughness-is-related-to-wettability>
- 20- Owens, Wendt, Rabel and Kaelble (OWRK) method (2021) <https://www.kruss-scientific.com/en/know-how/glossary/owens-wendt-rabel-and-kaelble-owrk-method>
- 21- Laurén, S. (2020, December 22). OWRK method – Owens, Wendt, Rabel and Kaelble model. *Biolin Scientific.* <https://www.biolinscientific.com/blog/owrk-method-owens-wendt-rabel-and-kaelble-model>
- 22- Makkonen, Lasse; Kurkela, Juha (2018). Another look at the interfacial interaction parameter. *Journal of Colloid and Interface Science*, (), S0021979718306593–. doi:10.1016/j.jcis.2018.06.015
- 23- Surface Tension, Surface Free Energy, and Wettability (2021) <https://www.nanoscience.com/techniques/tensiometry/surface-tension-surface-free-energy-and-wettability/>
- 24- A Guide to Surface Energy (2021) <https://www.ossila.com/pages/a-guide-to-surface-energy>

- 25- Surface Tension Components and Molecular Weight of Selected Liquids (2021)  
[https://www.accudynetest.com/surface\\_tension\\_table.html](https://www.accudynetest.com/surface_tension_table.html)
- 26- Dietrich, R. (2013, April 25). Calcite. Encyclopedia Britannica.  
<https://www.britannica.com/science/calcite>
- 27- Written in Chalk(2018)  
<https://www.biointeractive.org/classroom-resources/written-chalk>
- 28- Røyne, A., Bisschop, J., & Dysthe, D. K. (2011). Experimental investigation of surface energy and subcritical crack growth in calcite. *Journal of Geophysical Research: Solid Earth*, 116(B4).
- 29- Shyam, A., and E. Lara-Curzio (2006), The double-torsion testing technique for determination of fracture toughness and slow crack growth behavior of materials: A review, *J. Mater. Sci.*, 41(13), 4093–4104.
- 30- Wang, H., Zhao, F., Huang, Z. *et al.* Experimental Study of Mode-I Fracture Toughness for Layered Shale Based on Two ISRM-Suggested Methods. *Rock Mech Rock Eng* **50**, 1933–1939 (2017). <https://doi.org/10.1007/s00603-017-1180-8>
- 31- Fowell RJ, Hudson JA, Xu C, Chen JF, Zhao X. Suggested method for determining mode I fracture toughness using Cracked Chevron Notched Brazilian Disc (CCNBD) specimens. *Int J Rock Mech Min Sci Geomech Abstr.* 1995;32(1):57–64. [https://doi.org/10.1016/0148-9062\(94\)00015-U](https://doi.org/10.1016/0148-9062(94)00015-U)
- 32- Fowell RJ, Xu C, Dowd PA. An update on the fracture toughness testing methods related to the cracked Chevron-notched Brazilian disk (CCNBD) specimen. *Pure Appl Geophys.* 2006;163(5-6):1047–1057. <https://doi.org/10.1007/s00024-006-0057-7>
- 33- Fowell RJ, Xu C. The use of the cracked Brazilian disc geometry for rock fracture investigations. *Int J Rock Mech Min Sci Geomech Abstr.* 1994;31(6):571–579. [https://doi.org/10.1016/0148-9062\(94\)90001-9](https://doi.org/10.1016/0148-9062(94)90001-9).
- 34- Fowell RJ, Xu C. The cracked chevron notched Brazilian disc test- geometrical considerations for practical rock fracture toughness measurement. *Int J Rock Mech Min Sci Geomech Abstr.* 1993;30(7):821–824. [https://doi.org/10.1016/0148-9062\(93\)90029-D](https://doi.org/10.1016/0148-9062(93)90029-D).
- 35- Xu C, Fowell RJ. Stress intensity factor evaluation for cracked chevron notched brazilian disc specimens. *Int J Rock Mech Min Sci Geomech Abstr.* 1994;31(2): 157–162. [https://doi.org/10.1016/0148-9062\(94\)92806-1](https://doi.org/10.1016/0148-9062(94)92806-1).

- 36- Kuruppu, M. D., Obara, Y., Ayatollahi, M. R., Chong, K. P., & Funatsu, T. (2014). ISRM-suggested method for determining the mode I static fracture toughness using semi-circular bend specimen. *Rock Mechanics and Rock Engineering*, 47(1), 267-274.
- 37- Noël, C., Baud, P., & Violay, M. (2021). Effect of water on sandstone's fracture toughness and frictional parameters: Brittle strength constraints. *International Journal of Rock Mechanics and Mining Sciences*, 147, 104916.
- 38- Suggested ISRM. Methods for determining the uniaxial compressive strength and deformability of rock materials. *Int Soc Rock Mech*. 1979;16(2):137–140.
- 39- Descamps, F., Fay-Gomord, O., Vandycke, S., Schroeder, C., Swennen, R., & Tshibangu, J. P. (2017). Relationships between geomechanical properties and lithotypes in NW European chalks. *Geological Society, London, Special Publications*, 458(1), 227-244.
- 40- Nano and Pico Characterization Laboratory  
<https://npc.cnsi.ucla.edu/project/bruker-dimension-icon/>
- 41- AFM Modes  
<https://www.bruker.com/en/products-and-solutions/microscopes/materials-afm/afm-modes.html>
- 42- Contact Mode  
<https://www.bruker.com/en/products-and-solutions/microscopes/materials-afm/afm-modes/contact-mode.html>
- 43- TappingMode  
<https://www.bruker.com/en/products-and-solutions/microscopes/materials-afm/afm-modes/tapping-mode.html>
- 44- PeakForce Tapping  
<https://www.bruker.com/en/products-and-solutions/microscopes/materials-afm/afm-modes/peakforce-tapping.html>
- 45- PeakForce QNM  
<https://www.bruker.com/en/products-and-solutions/microscopes/materials-afm/afm-modes/peakforce-qnm.html>
- 46- AFM-nDMA  
<https://www.bruker.com/en/products-and-solutions/microscopes/materials-afm/afm-modes/afm-ndma.html>

47- FastForce Volume

<https://www.bruker.com/en/products-and-solutions/microscopes/materials-afm/afm-modes/force-volume.html>

48- Tunneling AFM (TUNA)

<https://www.bruker.com/en/products-and-solutions/microscopes/materials-afm/afm-modes/tuna.html>

49- DataCube Modes

<https://www.bruker.com/en/products-and-solutions/microscopes/materials-afm/afm-modes/datacube-modes.html>

50- Ebnesajjad, Sina (2011). *Handbook of Adhesives and Surface Preparation || Surface Tension and Its Measurement.* , ( ), 21–30. doi:10.1016/B978-1-4377-4461-3.10003-3

51- Pollock, H. M.; Maugis, D.; Barquins, M. (1978). *The force of adhesion between solid surfaces in contact.* , 33(9), 798–. doi:10.1063/1.90551

52- Lamprou, D. A., Smith, J. R., Nevell, T. G., Barbu, E., Willis, C. R., & Tsibouklis, J. (2010). Towards the determination of surface energy at the nanoscale: a further assessment of the AFM-based approach. *Journal of Advanced Microscopy Research*, 5(2), 137-142.

53- ADHESION CONTACT MECHANICS

<https://polymerdatabase.com/polymer%20physics/Adhesion%20Contact%20Mechanics.html#Beyond%20JKR>

54- Ciavarella, M.; Joe, J.; Papangelo, A.; Barber, J. R. (2019). *The role of adhesion in contact mechanics.* *Journal of The Royal Society Interface*, 16(151), 20180738–. doi:10.1098/rsif.2018.0738

55- Fluid Imaging

<https://www.nanophys.kth.se/nanolab/afm/icon/bruker-help/Content/Fluid%20Imaging/Fluid%20Imaging.htm>

56- Ortega, J.E., Barron-Gonzalez, M.P. , Gracia-Pinilla, M.A., Perez, E., Lopez-Aldrete, A. and Menchaca, J.-L. (2014) Biological Samples Observed in Vitro by Atomic Force Microscopy: Morphology and Elastic Properties. In: Mendez-Vilas, A., Ed., *Microscopy: Advances in Scientific Research and Education*, Formatex Research Center, Badajoz, 131-140.

- 57- IAZYKOV, M.; EROUEL, M.; VILLEY, R.; SOUTEYRAND, E.; TARDY, J.; PHANER-GOUTORBE, M.; SKRYSHEVSKY, V. A. (2012). AN AFM INVESTIGATION OF SURFACE ENERGY OF PENTACENE FILMS ON PARYLENE-C AND BENZOCYCLOBUTENE. *Functional Materials Letters*, 5(1), 1250016-. doi:10.1142/S1793604712500166
- 58- Royaux, Adeline; El Haitami, Alae; Fichet, Odile; Cantin, Sophie (2020). *Surface free-energy determination of copper wire using a large range of model liquids*. *SN Applied Sciences*, 2(1), 48-. doi:10.1007/s42452-019-1828-y
- 59- Geremia et al., (2021). Recent advances in characterizing water weakening and fluid rock interaction processes in porous rocks. *Applied Sciences* (Submitted)

# Appendices

The following data is for the contact angle measurements:

*Table 28- Contact Angle Measurements on Calcites*

Water	advancing angle		DIO	advancing angle		FORMA	advancing angle
sample 1	80.8		sample 1	71.1		sample 1	80.9
	80.7			74.5			79.8
	80.4			74.1			78
	77.2		sample 2	65.7		sample 2	62.7
	84.8			68.8			71.8
sample 2	69.4			73.3			69.3
	74.3		Mean	71.25		Mean	73.75
	74.5		sd	3.455864581		sd	7.092178791
Mean	77.7625		NB	6		NB	6
sd	4.887575356				NB Total		
NB	8				20		

Table 29- Contact Angle Measurements on Phosphatic Ciply Chalk

NAME	WATER	advancing angle	GLYC	advancing angle	DMSO	advancing angle	FORMA	advancing angle	DIO	advancing angle	C2				
C2	sample 1	85.2	sample 1	71.7	sample 1	60.7	sample 1	69	sample 1	71	3				
		86.1		75		62.1		80.8		71.9	2	5			
		87.5		68.1		58		71.7		75.6	4				
		83.6		79.7		58.2		63.9		74.6					
		81.8		70.7		61.1		63.9		76					
A7	sample 2	86	sample 2	76.4	sample 2	52.9	sample 2	71.7	sample 2	78.9	A7				
		82		72		54		76.8		72.5	3				
		90		75.6		52.3		65.4		70.1	2	5			
		83.2		73.9		51.4		67.4		65.5	4				
		88.8		74.7		55.3		70.9		72.4					
C5	sample 3	88.6	sample 3	73.6	sample 3	56.4	sample 3	70.6	sample 3	72.1	C5				
		85.4		73.4		57.6		71		74.4	2				
		83.6		69.7		61		68.4		74.9	4				
		77.2		69		57.5		73.1		68.5	1	3	5		
		83.1		71.3		56.3		66.9		70.5					
A4	sample 4	86.8	sample 4	81.8	sample 4	55.3	sample 4	65.4	sample 4	74.7	A4				
		80.9		80.4		54.5		66.2		77.4					
		85.5		75.8		51.6		70.2		78.8	2	4	5		
		85.5		81		56.4		62.9		77.2	3				
		87.4		80		55.1		66.7		75.3					
B2	sample 5	89.3	sample 5	X	B2										
		88.5		X		X		X		X	2	4			
		76.2		X		X		X		X	1	3	5		
		84.6		X		X		X		X					
		85.4		X		X		X		X					
E9	sample 6	91.5	sample 5	77.2	sample 5	57.7	sample 5	79.4	sample 5	70.8	E9				
		87.8		78.9		58.6		73.6		74.3	3				
		94.7		83.9		56.3		82.2		62.6	2	5			
		82.1		76.8		58		74.3		73.9	4				
		86.1		79.5		59.9		70		72.6					
B8	sample 7	91.2	sample 6	75.4	sample 6	55.1	sample 6	77.2	sample 6	70	B8				
		92.3		80.2		52.7		66.6		69.7	3				
		89.2		79.6		52.3		63.6		72.3	2	5			
		79.5		75.5		56.4		68.7		69.7	4				
		93.5		72.4		53.3		76.7		63.6					
	Mean	86.00286	MEAN	75.77333333	MEAN	56.26666667	MEAN	69.145	MEAN	73.615					
TOTAL NB	sd	4.260591	SD	4.115649975	SD	2.970467667	SD	4.4619414	SD	3.462167712					
155	NB	35	NB	30	NB	30	NB	30	NB	30					

Table 30- Contact Angle Measurements on Pure Resin

GLYC	advancing angle		WATER	advancing angle		WATER	advancing angle		DMSO	advancing angle		FORMA	advancing angle		DIO	advancing angle
sample 1	77.2		sample 1	80.9		sample 4	82.5		sample 1	55.1		sample 1	73.6		sample 1	79.9
	72.9			84.2			81.6			58.8			75.5			82.1
	65.7			84.6			74.3			48.2			78.4			78.2
	69.4			84.9			80			60.2			69.9			82.5
	73.1			80.5			82.6			55.7			66.4			72.3
	67.5			88			84			57.8			62.4			74.9
	72.3		sample 2	77.6		sample 5	76.2		sample 1	62.8		sample 1	61		sample 1	76.9
	72.4			83			74.4			56.3			71			63.1
	73.3			82.5			81.7			62.9			66.4			67
	78.1			74.4			75.9			61.3			72.2			68.5
	71.2			91			89			57.8			69.5			79.5
	75.1			76.1			82.3			63.4			72.5			81.7
71.7		76.5		81		62		67.4		78.2						
sample 2	78.1		sample 3	79.6		sample 6	74.3		sample 2	54.9		sample 2	74.8		sample 2	82.5
	75.2			76.2			76.5			51.3			71			82.1
	67.6			74.2			80.4			50			63.7			81.8
	67.5			81.4			74			47.5			76.5			75.9
	62.3		83.2		79		53		73		75.2					
	66.1		86.4		81.6		49		70.9		77.2					
	63		81.5		78.9		49.1		68.1		73.4					
	78.3		88.5		80.5		49.2		72.3		75.9					
	71.8		83.4		77.9		52.2		65.6		70.6					
	67.1				81.9		48.9		66.7		74.5					
sample 3	64.6							sample 3	52.5		sample 3	75.4		sample 3	73.6	
	68.5						50.6			62.5			68.7			
	68.5						50.7			69.5			72.2			
	68.9						50			68.1			76.6			
	64.1		TOTAL NB				55.4			70.9			71.7			
	64.5		187				55.2			60.7			76.8			
	70.4						59.6			67.7			72.4			
	71.5						55			68			74.9			
	77.3						57.7			68			70			
	64.6						59.9			71.2			77.7			
76.4						58.4		66.5		76.6						
64.9						54.8		73.8		65.7						
Mean	70.31714286							Mean	55.06285714			Mean	69.46		Mean	75.16571429
sd	4.758242738							sd	4.7581562			sd	4.406826256		sd	4.99987899
NB	35							NB	35			NB	35		NB	35



The following is the Data for the Static Contact Angle Measurements on Calcites:

Table 32- Brine Static Contact Angle Measurements on Calcites

Calcites	Contact Angle										
	Distilled water	0,075 NaCl	0,15 NaCl	0,3 NaCl	0,45 NaCl	1,05 NaCl	0,04 MgCl2	0,081 MgCl2	0,163 MgCl2	0,244 MgCl2	0,569 MgCl2
Sample 1	91.6	87.1	85	84.2	82.9	78.2	90.4	83.4	84.4	82.3	73.8
	85.8	86.7	88.5	86.9	80.8	81.5	87.9	84.2	78.8	79.4	72.9
	90.3	87.3	93.2	86.2	85.3	82.8	88.6	88.4	82	82.8	70.9
	84	89.6	88.7	84	84.3	76.8	91.1	87	85.1	83.7	76.4
	82.3	86.7	85.4	82	84.5	74	88.4	88.3	82.2	80.1	77
	Mean	86.8	87.48	88.16	84.66	83.56	78.66	89.28	86.26	82.5	81.66
SD	4.01185742	1.21326	3.294389	1.9437078	1.7686153	3.5564027	1.3881643	2.3298069	2.4698178	1.8311199	2.5209125
Sample 2	80	83.8	89.3	80.7	85.2	76.9	87.4	89.7	89.7	86	84
	83.4	86.3	80.2	82.2	88.9	81.2	89.3	89.7	91.8	82.3	84.5
	86	82.7	85.5	84.1	84.2	80.9	88.9	89.8	83.4	83.4	79.6
	87.6	87.8	87.3	83	85.1	81.1	90.8	88.4	86.1	80.4	77
	79.4	85.4	82.7	84	83.58	77	93	92.9	89.7	83	76.6
Mean	83.28	85.2	85	82.8	85.396	79.42	89.88	90.1	88.14	83.02	80.34
SD	3.60166628	2.013703	3.61801	1.4089	2.06956	2.257654	2.1229696	1.66883193	3.35007463	2.02533948	3.75473035

The following is the Data for the SCB tests:

Table 33- SCB Tests on Ciply Phosphatic Chalk

Name	Saturation	R'	a'saw	a'frac	a <sub>saw</sub>	a <sub>frac</sub>	R (radius)	S (spacing)	B (thickness)	V	β	Y'	F <sub>max</sub>	KIC	E	φ	γ	KIC <sub>avg</sub>	γ <sub>avg</sub>
PS1 L	DRY	2.3	0.9	0.95	1.05	1.1	2.45	2.45	2.6	21.23423	0.44898	3.238769	0.08	0.037807	1.185	φ	<b>0.603108</b>	0.052901	<b>1.023798</b>
PS2 M		2.1	0.675	0.675	1.025	1.025	2.45	2.45	2.5	17.0649	0.418367	3.019915	0.145	0.064145	1.185		<b>1.736116</b>		
PS3 S		2.35	0.825	0.8	0.925	0.9	2.45	2.45	1.8	15.3985	0.367347	2.731258	0.08	0.041656	1.185		<b>0.732171</b>		
PS4 L	Delonized Water	2.45	1	0.95	1	0.95	2.45	2.45	2.5	23.21551	0.387755	2.835306	0.0775	0.030989	0.495	0.379696	<b>0.969995</b>	0.027421	<b>0.846522</b>
PS5 M		2.1	0.65	0.7	1	1.05	2.45	2.45	2.4	16.37331	0.428571	3.089061	0.05	0.023854	0.495	0.400761	<b>0.574754</b>		
PS6 S		2.15	0.6	0.625	0.9	0.925	2.45	2.45	1.85	13.25942	0.377551	2.781379	0.06	0.031383	0.495	0.379052	<b>0.994818</b>		
cm										cm3	-	KN	MPa	-	J/m2	MPa	J/m2		

Table 34- SCB Tests on Obourg Chalk

Name	Saturation	R'	a'saw	a'frac	a <sub>saw</sub>	a <sub>frac</sub>	R (radius)	S (spacing)	B (thickness)	V	β	Y'	F <sub>max</sub>	KIC	E	φ	γ	KIC <sub>avg</sub>	γ <sub>avg</sub>
TEST	DRY	2.4	0.95	0.9	1	0.95	2.45	2.45	2.4	21.39069	0.387755	2.835306	0.2025	0.084344	5.48	φ	<b>0.64908</b>	0.084344028	<b>0.649079838</b>
OS1	DRY	2.2	0.85	0.825	1.1	1.075	2.45	2.45	2.3	17.20148	0.438776	3.162013	0.135	0.069607	5.48		<b>0.442074</b>		
OS2		2.4	0.9	0.875	0.95	0.925	2.45	2.45	2.45	21.84552	0.377551	2.781379	0.2	0.07899	5.48		<b>0.569295</b>		
OS3		2.25	0.7	0.65	0.9	0.85	2.45	2.45	2.2	17.28024	0.346939	2.64243	0.16	0.06409	5.48		<b>0.374772</b>		
OS4	Delonized Water	2.4	0.9	0.925	0.95	0.975	2.45	2.45	2.4	21.38169	0.397959	2.893037	0.125	0.053819	3.17	0.421349	<b>0.456855</b>	0.050350892	<b>0.402286953</b>
OS5		2.3	0.85	0.85	1	1	2.45	2.45	2.5	20.45503	0.408163	2.954574	0.105	0.044887	3.17	X	<b>0.317802</b>		
OS6		2.4	0.95	9.25	1	9.3	2.45	2.45	2.5	19.15072	3.795918	233.7162	X	X	3.17	0.418745	<b>X</b>		
OS19		2.25	0.8	0.8	1	1	2.45	2.45	2.45	19.18878	0.408163	2.954574	0.12	0.052347	3.17	0.423774	<b>0.432204</b>		
OS7	NaCl	2.45	0.95	0.95	0.95	0.95	2.45	2.45	2.65	24.60844	0.387755	2.835306	0.105	0.039608	2.76	0.41731	<b>0.284203</b>	0.036989623	<b>0.259987456</b>
OS8		2.2	0.8	0.775	1.05	1.025	2.45	2.45	2.45	18.34169	0.418367	3.019915	0.0825	0.037241	2.76	0.422215	<b>0.251251</b>		
OS9		2.3	0.85	0.85	1	1	2.45	2.45	2.4	19.63683	0.408163	2.954574	0.0825	0.036738	2.76	0.413824	<b>0.244508</b>		
OS10	MgCl2	2.2	0.7	0.725	0.95	0.975	2.45	2.45	2.45	18.36007	0.397959	2.893037	0.1	0.042176	3.78	0.415459	<b>0.235297</b>	0.04947669	<b>0.25638078</b>
OS11		2.2	0.7	0.75	0.95	1	2.45	2.45	2.4	17.97637	0.408163	2.954574	0.1275	0.056777	3.78	0.425532	<b>0.426406</b>		
OS12		2.25	0.75	0.8	0.95	1	2.45	2.45	2.25	17.62235	0.408163	2.954574	0.06	0.0285	3.78	0.430334	<b>0.107439</b>		
OS13	CaCl2	2.2	0.7	0.7	0.95	0.95	2.45	2.45	2.5	18.74414	0.387755	2.835306	0.11	0.043984	3.75	0.421784	<b>0.257944</b>	0.045833001	<b>0.285410655</b>
OS14		2.15	0.7	0.7	1	1	2.45	2.45	2.25	16.10101	0.408163	2.954574	0.0825	0.039187	3.75	0.421732	<b>0.204752</b>		
OS15		2.4	0.9	0.9	0.95	0.95	2.45	2.45	2.3	20.49941	0.387755	2.835306	0.125	0.054328	3.75	0.425972	<b>0.393536</b>		
Ionic Strength	0.598	cm								cm3	-	KN	MPa	-	J/m2	MPa	J/m2		

The following is the Data for the Roughness Measurements:

For Obourg Chalks:

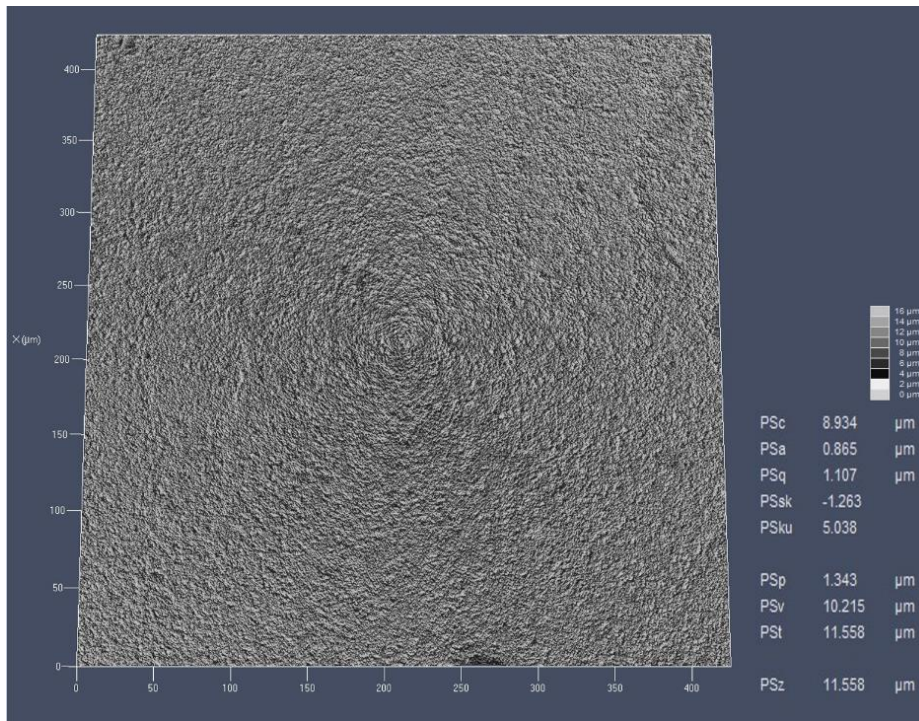


Figure 50- Roughness Measurements of OB Chalk Sample 1

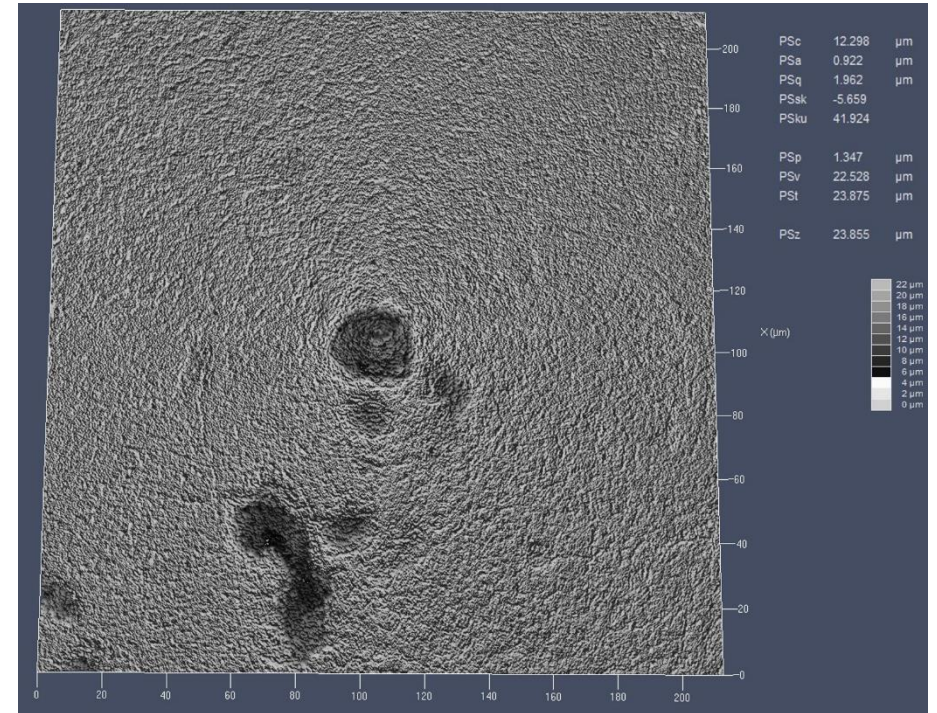


Figure 51- Roughness Measurements of OB Chalk Sample 2

For Ciplly Phosphatic Chalks:

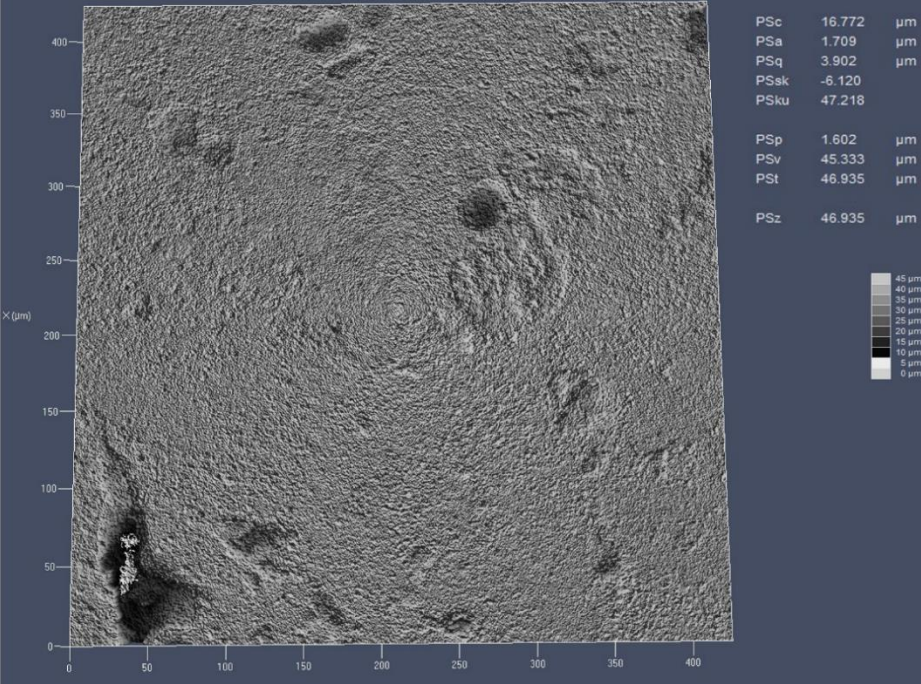


Figure 52- Roughness Measurements of PH Chalk Sample 1

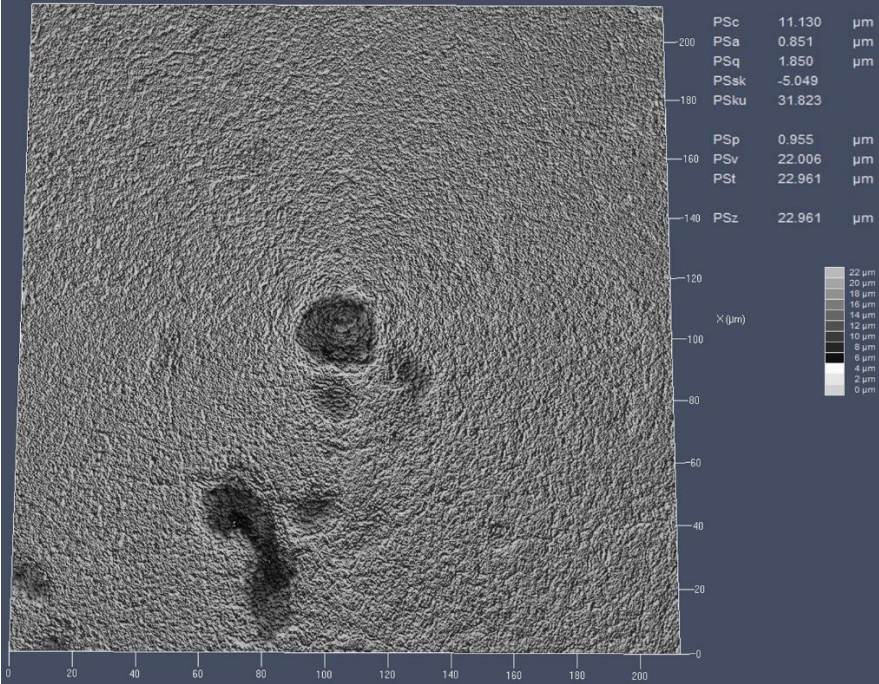


Figure 53- Roughness Measurements of PH Chalk Sample 2

For Calcites:

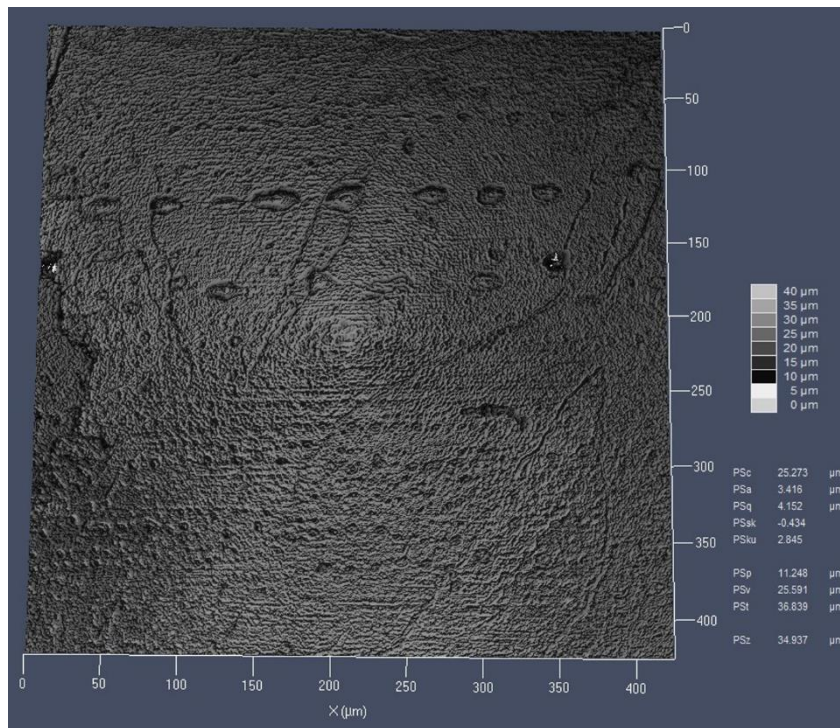


Figure 54- Roughness Measurements of Calcite 1

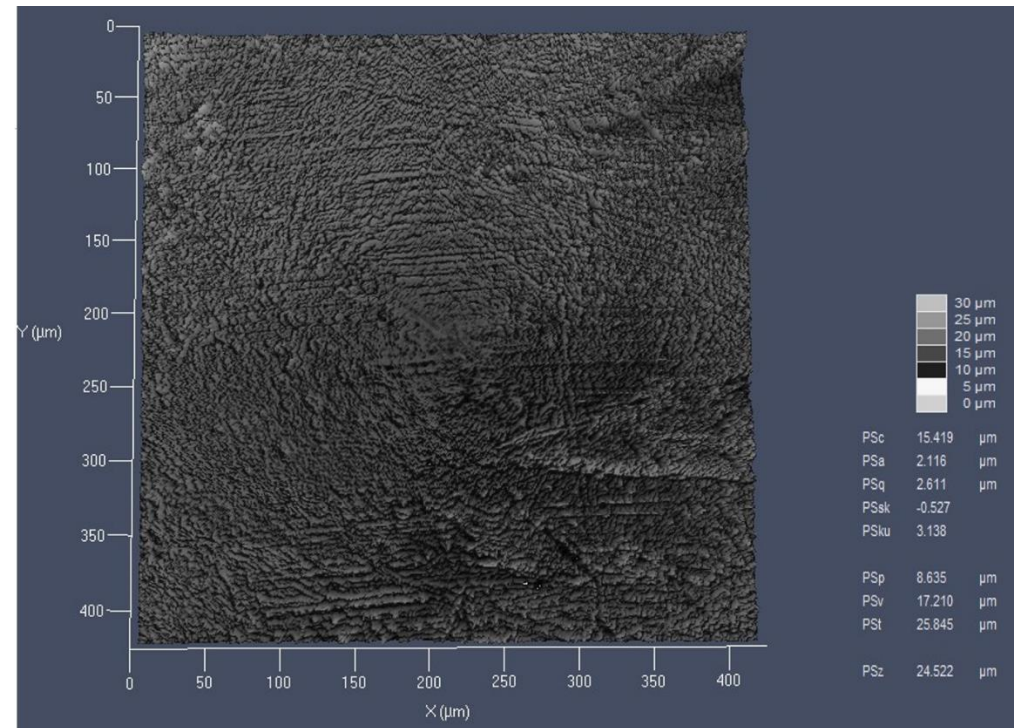


Figure 55- Roughness Measurements of Calcite 2